Graduation thesis: Validating and developing measurement techniques to assess patellofemoral instability using dynamic Computed Tomography.

Technical Medicine, MII, Graduation thesis, 24-05-2023

H.H. van Dijk BSc

Graduation committee

Chairman: Prof.dr.ir. N. Verdonschot

Medical supervisor: Dr.ing. S.A.W van de Groes

Technical supervisor UT: Prof.dr.ir. N. Verdonschot

Daily supervisor: ir. M.R. Boot

Process supervisor: Drs. R.M. Krol

External member: Dr.ir. L. Alic

Radboudumc university medical center

UNIVERSITY OF TWENTE.

Preface

Voor u ligt mijn afstudeerthesis getiteld ‘Validating and developing measurement techniques to assess patellofemoral instability using dynamic Computed Tomography’. Deze thesis is geschreven ter afronding van de master Technische Geneeskunde met als specialisatie richting ‘Medical Imaging and Interventions’. De afgelopen 13 maanden heb ik hiervoor stage gelopen bij het Radboudumc te Nijmegen, op de afdeling Orthopedie en het Orthopeadic Research Lab.

Gedurende mijn opleiding, en met name de afgelopen 2 jaar heb ik de kans gehad om mezelf op meerdere vlakken te ontwikkelen. Dit had enerzijds betrekking op mijn technische en medische ontwikkeling, maar ook heb ik mezelf als persoon mogen ontwikkelen. Over het algemeen heb ik dit dan ook als zeer waardevolle periode ervaren.

Toch is dit niet altijd makkelijk geweest. Gedurende het afgelopen jaar liep ik steeds meer aan tegen de vraag: ‘Wat wil ik hierna gaan doen?’. Ik heb hierbij regelmatig mijn twijfels en onzekerheden gehad over wat de juiste keuze zou zijn. Hierbij heeft het mij heel erg geholpen dat ik deze twijfels kon delen met de mensen om mij heen.

Ik wil dan ook iedereen die een rol heeft gehad in het succesvol afronden van deze periode bedanken. Nico en Sebastiaan, jullie hebben mij niet alleen op technisch en medisch vlak ondersteund, maar stonden ook open voor mijn twijfels en onzekerheden. Miriam, als dagelijks begeleider was jij de eerste bij wie ik altijd terecht kon, wat soms gepaard ging met de nodige tranen, en die altijd bereid was om mij verder te helpen. Ruby, als procesbegeleider was jij degene die me hielp mezelf beter te begrijpen en meer en meer naar mijn gevoel te luisteren. Alle vier bedankt hiervoor. Tevens ben ik erg dankbaar voor alle mensen van de afdeling Orthopedie, door jullie heb ik mezelf klinisch kunnen ontwikkelen en voelde ik me erg welkom. Daarnaast de mensen van het Orthopeadic Research Lab, jullie stonden altijd open voor hulp maar ook voor een erg gezellig tijd. Tot slot ben ik erg dankbaar voor de onvoorwaardelijke steun van mijn vrienden en familie.

Abstract

Introduction : A prevalence of 6 to 77 per 100.000 is estimated for acute traumatic patellar dislocations, mostly affecting adolescents. When some predisposing factors, or anatomical variations, are present, there is an increased risk for patellar luxation. Some important predisposing factors are patella alta, trochlear dysplasia and an increased tibial tuberosity-trochlear groove (TT-TG) distance. The use of dynamic imaging, such as four dimensional computed tomography (4D CT) could help in understanding the movement of the knee. This research was conducted to obtain more knowledge regarding the current patella alta measurements, the Insall Salvati and Caton Deschamps index (CDI), and the relationship between the movement of the patella in relation to the trochlear groove.

Methods: Two databases, one of healthy volunteers and one of patients with patellofemoral instability (PFI) were used for this research. To assess the current patella alta measurement simulated X-rays were created on which the indices were measured. The novel method looked at the patella lateralization in relation to the trochlear groove by determining both condyles, the trochlear groove and the patellar projection point. The distance between the patellar projection point and trochlear groove was determined for further statistical analysis.

Results: Regarding the patella alta measurements, not many statistical differences were found. For both indices a difference was found for the effect of muscle tension. For the CDI a change of tibiofemoral flection angle and a adduction of 5° was found to be statistically different. With regard to the patellar lateralization, a statistical difference was found between the healthy volunteers and patients with PFI throughout the first half of the trochlear groove. When looking at individual patients some showed an aberrant tracking but some showed a normal tracking as well.

Conclusion: Based on this research it can be concluded that both the Insall Salvati and the Caton Deschamps index are robust measurement methods for patella alta. Besides, the distance between the patellar projection point and trochlear groove showed increased

lateralization in patients with PFI. Future research should focus on optimizing and elaborating this workflow to include other predisposing factors. This will hopefully lead towards a patient specific guideline for the diagnosis and treatment of patients with PFI.

Contents

Chapter 1: General introduction

The broad term patella instability includes patellar dislocation, patellar subluxation and patellar instability, and represents up to 3% of clinical presentations concerning the knee.[1,2] When looking at acute traumatic patellar dislocation a prevalence of 6 to 77 per 100.000 is estimated. Primary dislocation occurs mostly in adolescents, most often as a result of trauma during physical activity. A dislocation occurs when the patella moves to far lateral, and out of the trochlear groove. In the healthy knee, the medial patellofemoral ligament (MPFL) prevents the patella from dislocating laterally (Figure 1).

Figure 1. Visualization of the anatomy of the knee, showing the MPFL.[3]

The MPFL contributes up to 50 to 60% of the medial restraining force, Figure 2A of the patella, making it the most important soft tissue restraint.[4] Due to the traumatic force, the MPFL is generally injured after the dislocation (Figure 2B). This damage contributes to a higher incidence of reluxation.[2]

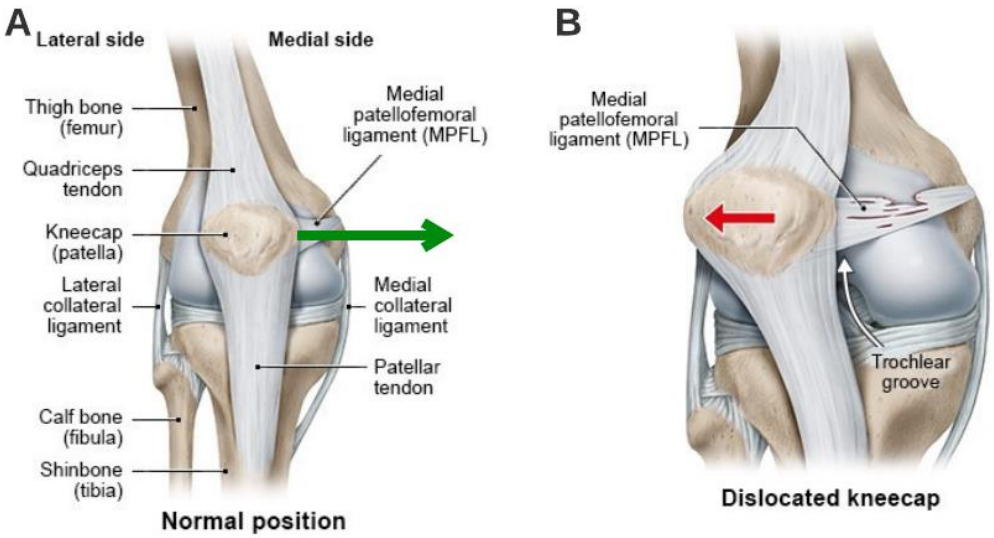

Figure 2. Function of the MPFL. A. The restraining force of the MPFL is pulling the patella medially (green arrow). B. A lateral pulling force (red arrow) can result in damage or tearing of the MPFL.[5]

Predisposing factors

There are some predisposing factors, or anatomical variations, that are associated with an increased risk for patellar luxation. The most common predisposing factors are patella alta, trochlear dysplasia, an increased tibial tuberosity-trochlear groove (TT-TG) distance and an increased Q-angle. A combination of multiple predisposing factors, will further increase the chance of patellar reluxation.[6]

Patella alta

Patella alta, also known as a high-riding patella, indicates that the patella is positioned higher than normal in relation to the femur. The incidence of patella alta varies throughout multiple studies. An incidence of 36% and 53%, in patients with patellar instability, was described in two different studies.[7,8] Due to this high placement, during extension, the patella is located at the shallow part of the trochlear groove. Therefore, the bony restriction of the trochlear groove is less pronounced. Besides that, patients with patella alta experience patellar instability throughout a wider range of motion. In the healthy knee, the patella engages with the trochlear groove around a flexion angle of 20-30°.[9] In patients with patella alta, a higher flexion angle is required to obtain this engagement, resulting in a higher risk of patellar dislocation (Figure 3).

Currently, the measurement of patella alta is conducted on a true lateral X-ray with a knee flexion of 30°. The knee position in this X-ray is often not optimal, which could affect the current measurement methods. More detailed information about the patella alta and its measurement is provided in chapter 2.

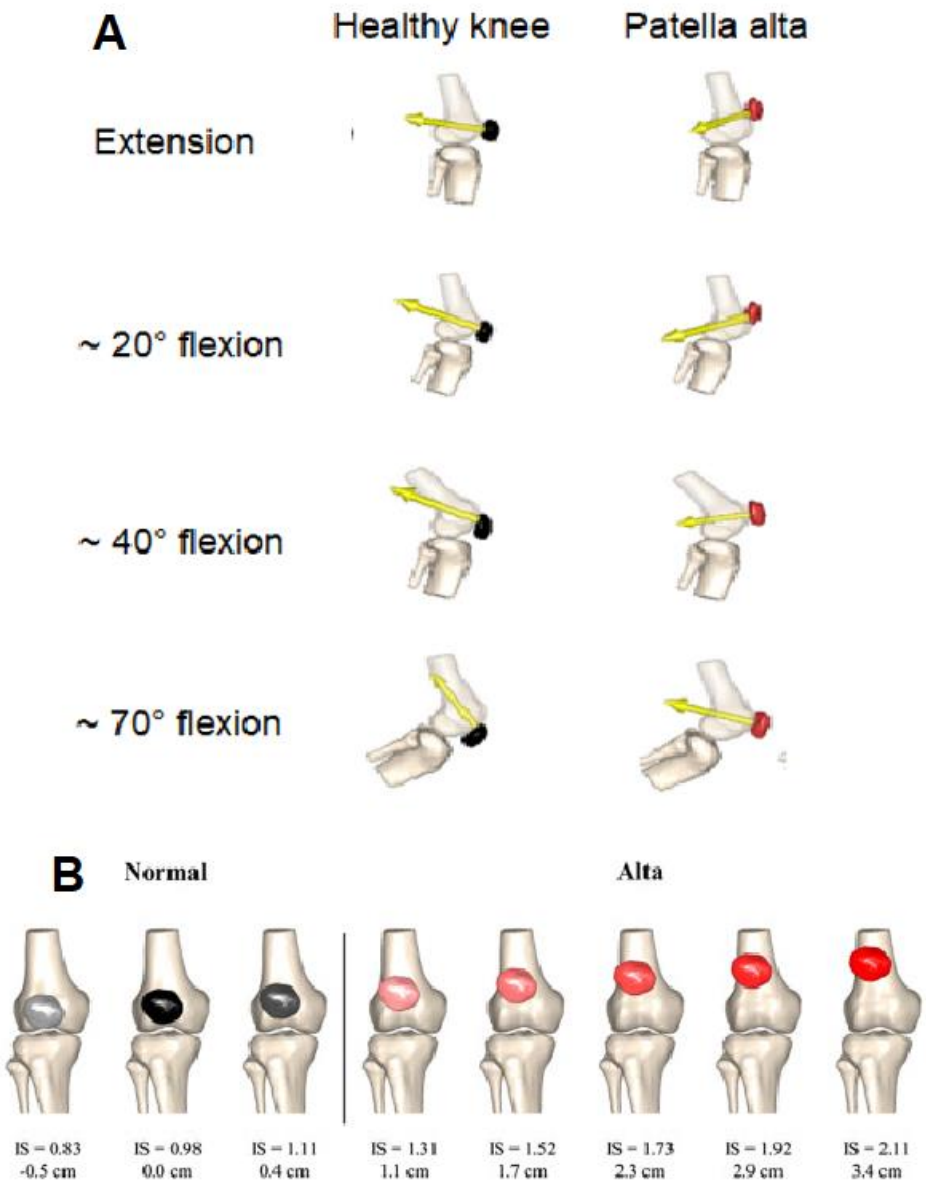

Figure 3. Effect of patella alta. A.Sagital view, the left row represents the healthy knee in which the patella (black) is located in front of the trochlear groove around 20°. The right row represents patella alta, in which a high position of the patella (red) is visible in 20°, the patella engages with the trochlear groove around 40°. B. frontal view of the position of the patella in relation to the trochlear groove. [10]

Trochlear dysplasia

Trochlear dysplasia is known as a condition where the trochlear groove is shallow or abnormally shaped. Some form of trochlear dysplasia is very common in patients with patellar luxations. Dejour et al. described that 96% of patients with a true luxation, have some form of trochlear dysplasia, in comparison to only 6.5% of the healthy population. The severeness of trochlear dysplasia is currently indicated with the Dejour classification, which ranges from A to D in which D is most severe (Figure 4).[11]

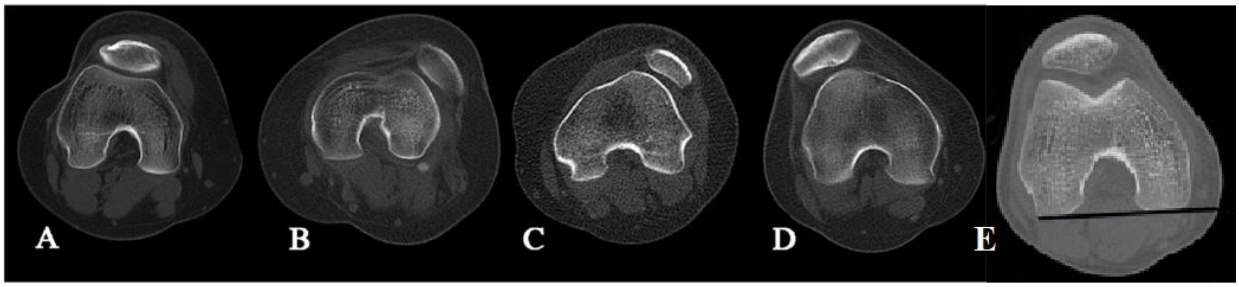

Figure 4. Overview of different trochlear grooves. A. Dejour type A dysplasia. B. Dejour type B dysplasia. C. Dejour type C dysplasia. D. Dejour type D dysplasia. E. healthy trochlear groove.[12,13]

Trochlear dysplasia results in a reduction of groove depth. Therefore, the bony support and restriction will be minimized, and the patella is more prone to dislocate. When looking at the trochlear depth, a depth below 4 mm was found to be pathological, in contrast to a mean trochlear depth of 7.8 mm in healthy controls. A pathological trochlear depth was present in 85% of the patients in comparison to only 3.5% of the healthy controls.[14] Besides that, a smaller lateral femoral condyle is often present in patients with trochlear dysplasia.[15]

TT-TG distance

The TT-TG distance is the distance between the deepest part of the trochlear groove and the tibial tubercle, and is currently used to determine the lateralization. An enlarged TT-TG distance, in this case above 15 mm, was found in 71.5% of patients in comparison to only 24.5% of healthy controls. Currently, the TT-TG distance is measured on axial slices of a CT or MRI, with the knee in full extension, Figure 5A shows this method in the frontal plane. With this method no information is obtained regarding the lateralization during the movement of the knee. An increased TT-TG distance is associated with an increased lateral pulling force, Figure 5B. More elaborate information about the measurement method of the TT-TG distance is provided in chapter 3.

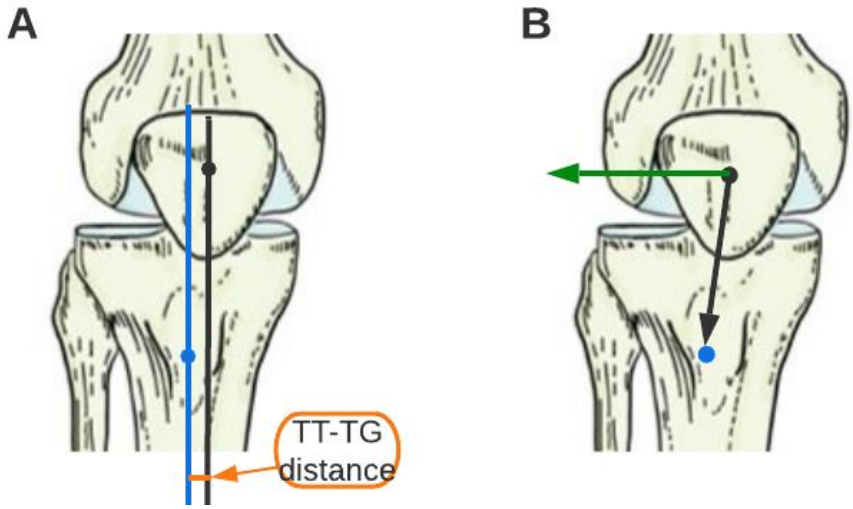

Figure 5. TT-TG measurement method. A. Distance between the trochlear groove (black dot) and tibial tuberosity (blue dot). B. The pulling force of the patella tendon (black arrow), and its resolved lateral dislocating force(green).[16]

Q-angle

The Q-angle is calculated using the tibial tubercle, midpoint of the patella and the anterior superior iliac spine; the measurement method is visualized in Figure 6A. In comparison to the other predisposing factors, the Q-angle is less used in daily clinical practice and its clinical relevance is doubtful. A literature review by Skouras et al.[17] showed that the standardized Q-angle differs between man and woman, but also between races. Normal values were described to vary between 0 and 28°, but are mostly described between 10 and 20°. An increased Q-angle can result in a greater lateral force acting (blue arrow Figure 6B) on the patella due to the altered pulling direction of the quadriceps muscles (green arrow Figure 6B), leading to potential patellofemoral instability problems.[18]

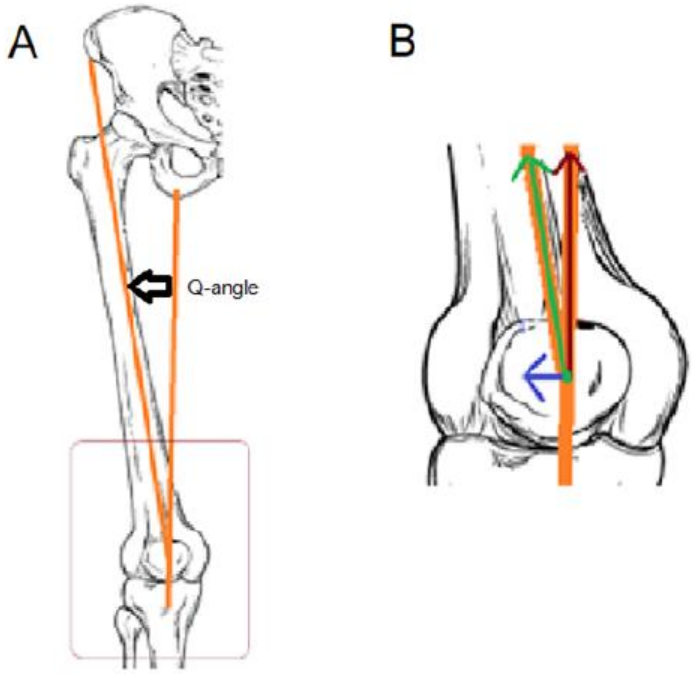

Figure 6. A represents the calculation method for the q-angle. B The quadriceps force (green arrow) can be resolved in a cranial force (red arrow) and a lateral pulling force (blue arrow).[19]

Imaging techniques

A conventional X-ray is used as a starting point for patients presenting with patellofemoral instability. Based on this X-ray, the presence of patella alta and trochlear dysplasia can be determined. A conservative policy can be followed, if it is the first location or when there is no indication that these predisposing factors are present, Otherwise, there is an indication for further investigation, such as a CT or MRI scan. This scan can be used to rule out or confirm the presence of the predisposing factors. Besides, an MRI scan is indicated to determine if there is any damage to the MPFL.[20]

Treatment options

After recurrent patellar luxations multiple surgical treatments are available to regain stability and prevent future luxations. Treatment options are MPFL reconstruction, and surgical interventions to minimize the effects of the predisposing factors, such as tuberosity distalization and lateralization, and trochleoplasty.

MPFL reconstruction

MPFL reconstruction is often performed in combination with another intervention to minimize the effects of these predisposing factors. Isolated MPFL reconstruction is only indicated when there are no predisposing factors.[21] In both cases, a similar operation technique can be used, but the optimal operation technique is still questioned. Decisions will be made with regard to the graft choice, placement and tension, and a static or dynamic reconstruction.[22]

Tuberositas distalization or medialization

As an addition to the MPFL reconstruction a tuberositas distalization and/or medialization is often performed.[4] Tuberositas distalization can be used to minimize the effects of patella alta, and tuberositas medialization can be applied to minimize the effects of an increased TT-TG distance and an increased Q-angle. Both techniques require an osteotomy of the anterior tibial tuberosity, which is subsequently moved. The amount of medialization and distalization is based on a preoperative assessment of the available imaging. This is often around 10 mm of distalization and 3-10 mm of medialization.[23]

Trochleoplasty

Trochleoplasty is a technique in which the shape of the trochlea is surgically adjusted. The technique is more invasive and technically demanding and only indicated in patients with severe dysplasia. Over the past decades, multiple different techniques have been developed. The different techniques can be divided globally into 2 groups, the trochlear deepening technique (Figure 7) and an approach to elevate the lateral trochlear facet.[24] The actual effect of this procedure is very uncertain, due to the fact that it is most often performed in combination with other surgical interventions. Besides, mixed subjective satisfaction rates between 65 and 75% have been described. Patients' satisfaction is reduced due to persistent complaints such as pain, stiffness and functional impairment.[25]

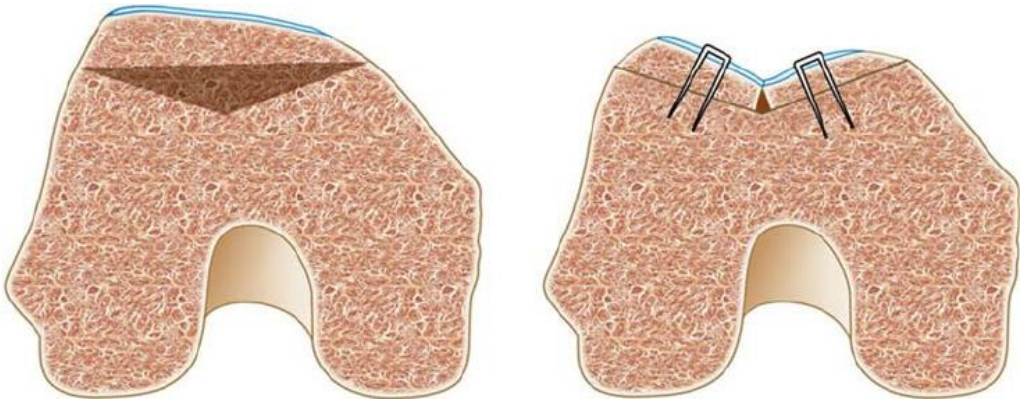

Figure 7. Sulcus deepening trochleoplasty schematic model. Cancellous bone from the trochlear undersurface is removed to allow modelling (gray zone). The bone – cartilage flap is then modelled, and fixation is achieved with staples.[26]

The aim of this thesis

To better understand the effect of the known predisposing factors and improve the current diagnostic and surgical techniques, imaging techniques that acquire data during motion are desirable. This could be achieved with the use of four dimensional computed tomography (4D CT) data. In a previous study by Dunning et al.[27] normative tibiofemoral and patellofemoral kinematics were evaluated.

This thesis was divided into two chapters. In chapter 2, 4D CT data was used to determine the robustness of different patella alta measurements. In chapter 3 a novel method to visualize patellar lateralization was introduced.

Chapter 2: Robustness of patella alta measurements

Introduction

Patella alta is one of the key risk factors for patellofemoral pain and instability, due to patellofemoral malalignment and a reduction of patellofemoral engagement in knee extension.[28,29] The incidence of patella alta is up to 75%[30] in patients with episodic patellar dislocation, in comparison to only 3% of the healthy controls[14]. Patients with patellar instability caused by patella alta can be treated via surgical correction. Therefore, usually, the patellar height is assessed in patients with patellar instability. Multiple methods can be used to determine if a patella alta is present.[31] Three methods which are often used are the Caton-Deschamps index (CDI), the Insall-Salvati index (ISI), and the Blackburne-Peel index, these are visualized in Figure 8.[32] Normal values for these indices are described as 0.6-1.2 for the CDI, 0.8-1.2 for the ISI and 0.8-1.0 for the BPI.[33]

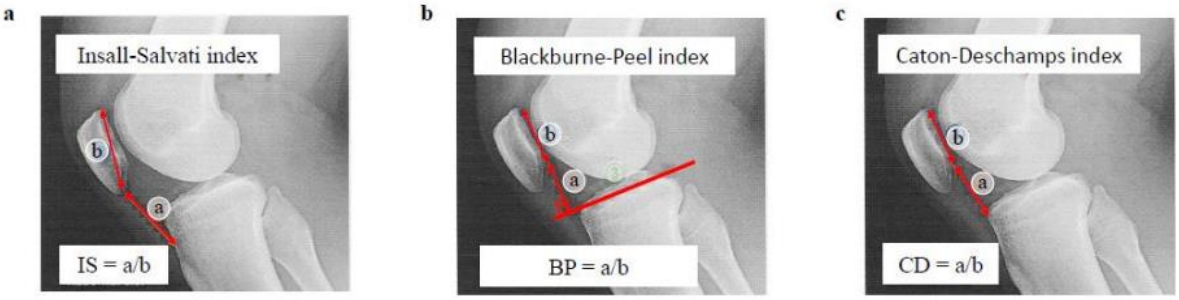

Figure 8. Overview of the three different measurement techniques for the patellar height.[32]

To calculate these indices a non-weight bearing true lateral X-ray with the knee in 30° flexion is made.[31] In practice, it is quite difficult to make an X-ray that is truly lateral. Another uncertainty is the degree of flexion of the knee. Patients can slightly move their knee, altering the flexion angle in which the X-ray is taken. Yet, the effect of these uncertainties on the measured indices is unknown although errors might lead to incorrect surgical planning.

Previous research conducted by Narkbunnam et al.[34] described that variation of the tibiofemoral angle from 0°, 30°, and 60° did not result in clinically relevant differences. Increasing the tibiofemoral angle from 0° to 30° resulted in an average increase of 0.071 for the ISI and an average decrease of 0.047 for the CDI. Further increasement of the tibiofemoral

angle from 30° to 60°, caused an average reduction of 0.018 for the ISI and 0.059 for the CDI. It was also described that there was a difference in CDI, Blackburne-peel index and modified ISI, between weight bearing and non-weight bearing X-rays. During this research goniometric rulers were used to verify the correct tibiofemoral angle, resulting in a low reliability. Besides this, no research was previously conducted to evaluate the effect of endo-/exorotation and ab-/adduction.

The first aim of this study was to first verify the influence of positional errors in flexion and extension on the patella alta measurements. The second aim was to assess the effect of positional errors in endo- and exorotation, and ab- and adduction on the measured CDI and ISI. Also, the effect of muscle tension will be assessed to evaluate the differences between the measured indices and the clinical cut-off values.

Methods

We used 4D CT scans, which makes it possible to obtain CT scans during motion. With the use of this technique, multiple different CT scans are made during the movement of the knee, to simulate the different errors which can be made, when the X-ray is made.

Data acquisition

A database with static and dynamic CT scans of 100 healthy volunteers was used for this research. The study was approved by the ethics committee Oost-Nederland. The most important inclusion criterion of this database was the absence of any knee complaints and previous knee surgeries. All volunteers had undergone a conventional 3D CT scan and a 4D CT scan on a Canon Aquilion One Genesis scanner. At first the conventional 3D CT was made of both knees in full extension, Figure 9a. Then, the 4D CT scan was made, acquiring 41 scans during an active flexion-extension-flexion movement (90° of flexion to full extension) in roughly 10 seconds, (Figure 9b,c).

Figure 9. a) 3D or static CT, with knees fully extended; b) 4D or dynamic CT with the knees in 90° flexion; c) 4D or dynamic CT with the knees fully extended.[27]

The next step was to process this data and to determine the tibiofemoral angle, using the anatomical femoral coordinate frame (AFCF) and the anatomical tibial coordinate frame (ATCF). To obtain these coordinate frames, first an automatic bone segmentation neural network was used to create masks of the tibia, femur and patella.[35] These masks were subsequently used to calculate the transformation from the conventional CT to the 4D CT, using a coherent point drift algorithm followed by an intensity-based image registration with the Elastix toolbox. These transformations were used to make it possible to use the field of view (FOV) of the static CT scan, which was necessary to calculate the AFCF.[27] These coordinate frames were calculated using the ERCKneeReferenceFrames, which was based on the method of Miranda et al.[36]. Figure 10 visualizes the segmentations of the femur, patella and tibia and their corresponding coordinate systems. An overview of the steps taken to determine the transformations from the static to the dynamic CT scan is shown in Figure 11.

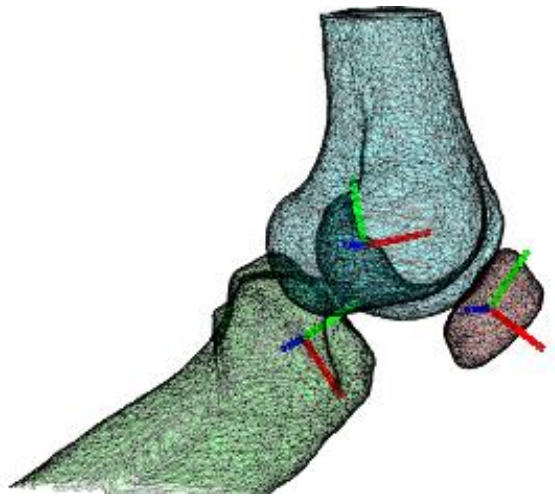

Figure 10. Overview of the segmented bones, femur (blue), tibia (green), patella (red) and their corresponding reference frames.

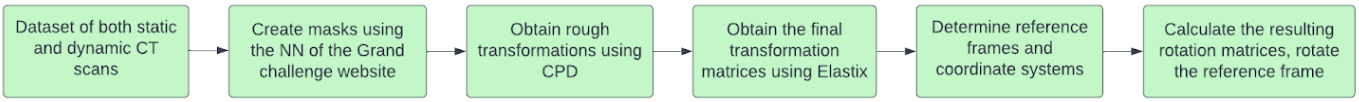

Figure 11. Overview of steps taken to determine the transformations from the static to dynamic CT scan. CT, computed tomography; NN, neural network; CPD, coherent point drift.

Patient Inclusion

A total of 47 knees from 35 participants were selected from the database and included in this study. This selection was based on the following inclusion criteria:

- Maximum of 5° deviation, from the chosen tibiofemoral angles of 15°, 30°, and 45°
- The minimal flexion angle reached with 4DCT scanning deviates ≤ 5° from the extension angle with 3D CT scanning
- Visibility of the tibial tuberosity
- Visibility of the whole patella

Calculation CDI and ISI

To create the simulated X-rays with the different positioning errors, average intensity projections were used. A total of thirteen projections, table 1, were created per knee to calculate the effect of rotational errors on the CDI and the ISI.

Table 1. Overview of the used simulated X-rays.

Flexion angle	Used CT scan	Simulated malpositions
0	Static and Dynamic	Not used
15	Dynamic	Not used
30	Dynamic	4 projections with medial-lateral deviation
		4 projections with anterior-posterior deviation
45	Dynamic	Not used

The projections were made using a combination of Matlab R2022a (Mathworks, Natick, Massachusetts,USA) and Python (Python Software Foundation, https://www.python.org/). To create the projections, first, the femoral anatomical reference frame of each CT scan was transformed to the world coordinate system (WCS). These transformations were then used to obtain a true lateral position of the femur in the CT scan. Subsequently, the CT scans were divided into left and right, and a projection was made for each knee. A true lateral projection was made for the static scan and the dynamic CT data at tibiofemoral angles of 0°, 15°, 30 °,

and 45°. Besides that, the dynamic scan with a tibiofemoral angle of 30° was used to create 8 deviated lateral projections. A deviation of 5° and 10° in both medial-lateral and anterior-posterior direction were made, to represent ab-/adduction and endo-/exorotation. This deviation was chosen based on a research of Wang et al., which described that based on the conventional lateral position, the X-ray of the standard lateral knee joint had a deviation between -10° and +7°.[37] An example of these average intensity projections is represented in Figure 12. It can be seen that in the right image, the projection of the femoral condyles is not optimal (green arrow). Besides, due to the rotation the fibula is rotated behind the tibia, making it less visible (blue arrow).

To determine the effect of muscle tension the simulated X-rays of the static scan and the dynamic scan with a flexion angle of 0° were used. During the static CT scan the muscles of the volunteer were relaxed, making it passive extension. During the dynamic CT scan the volunteer actively extended the knee, which required muscle activation.

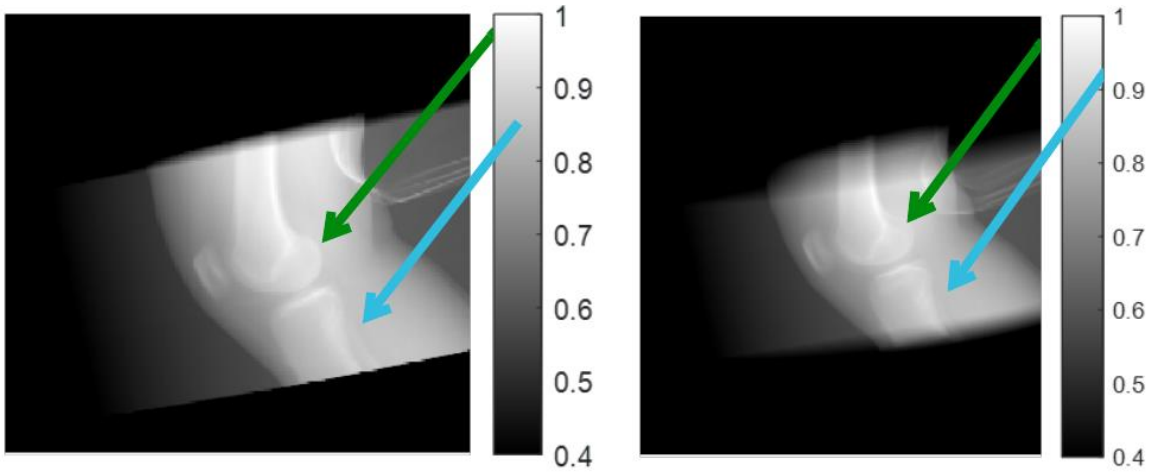

Figure 12. An example of an average intensity projection with a tibiofemoral angle of 30°. Left true lateral and right with an endorotation of 10°. The green and blue arrows indicate the visual differences between the images.

For the calculation of the CDI and the ISI a total of 6 different points were manually selected on each projection (Figure 13). The selection of these points was discussed with an experienced orthopaedic surgeon prior to the selection. The CDI is calculated by C/D, with a normal range of 0.6-1.2, and the ISI is calculated by A/B, with a normal range of 0.8-1.2.

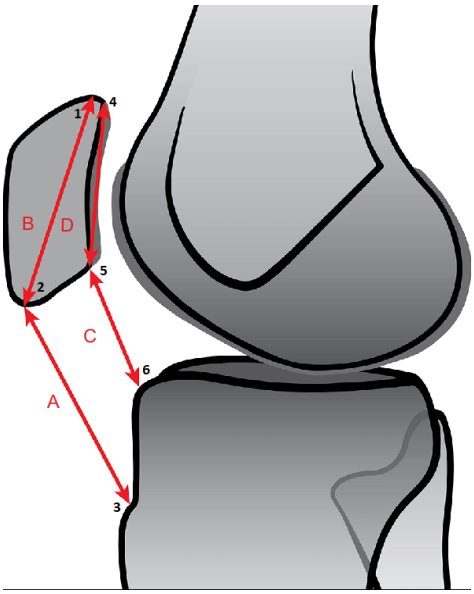

Figure 13. Calculation of Insall Salvati Index: A/B, and Caton Deschamps Index: C/D. Points selection: 1. superior aspect of the patella 2. inferior aspect of the patella, 3. tuberositas tibiae, 4. superior aspect of the articular surface, 5. inferior aspect of the articular surface, 6. anterior corner of the superior tibial joint surface

Statistical analysis

The measurements were divided into different subgroups for further analysis. These subgroups were composed to determine the effect of muscle tension, incorrect tibiofemoral angle, ab-/adduction, and endo-/exorotation. SPSS software (version 27.0, SPSS Inc., Chicago, IL, USA) was used to execute the statistical analysis. For all subgroups boxplots were made to visualize the different indices. First, the Kolmogorov-Smirnov test was used to check for a normal distribution. Subsequently, a paired t-test was used to determine if any significant differences were present, indicating that an effect of rotational errors is present. A total of 22 t-tests were executed, therefore a Bonferroni correction was made, resulting in a p-value below 0.002.

Results

Of the 35 included participants, 6 were men and 29 were women. The mean age was 24.5 years (19-32). The difference between the tibiofemoral angle in the static and dynamic scan averaged 1.26° (range: 0-4.9°). The differences between the actual and the desired tibiofemoral angles of 15°, 30° and 45° were 0.69° (0-2.6), 0.81° (0-3.2), and 0.78° (0-2.3), respectively.

Caton Deschamps Index

The boxplots representing the CDI of the four subgroups are visualized in Figure 14. The median of the static CDI is 1.01 (IQR 0.84 and 1.08) and the median of the dynamic CDI is 1.23 (IQR 1.09 and 1.35), resulting in a significantly higher CDI in the dynamic scan in relation to the static scan (p-value <0.001). The median of the dynamic CDI with a flexion angle of 15° is 1.06 (IQR 0.98 and 1.21) and the median of the dynamic CDI with a flexion angle of 30° is 0.99 (IQR 0.90 and 1.05). This leads to a significantly higher CDI for a flexion angle of 15° in comparison to 30° of flexion (p-value <0.001). An adduction of 5°, with a median of 1.01 (IQR 0.95 and 1.13), resulted in a significantly higher CDI in relation to the true lateral projection (p-value <0.001). A flexion angle of 45°, in comparison to a flexion angle of 30° did not result in a statistical difference (p = 0.174). Besides the adduction of 5° all other lateral deviations were not statistically different.

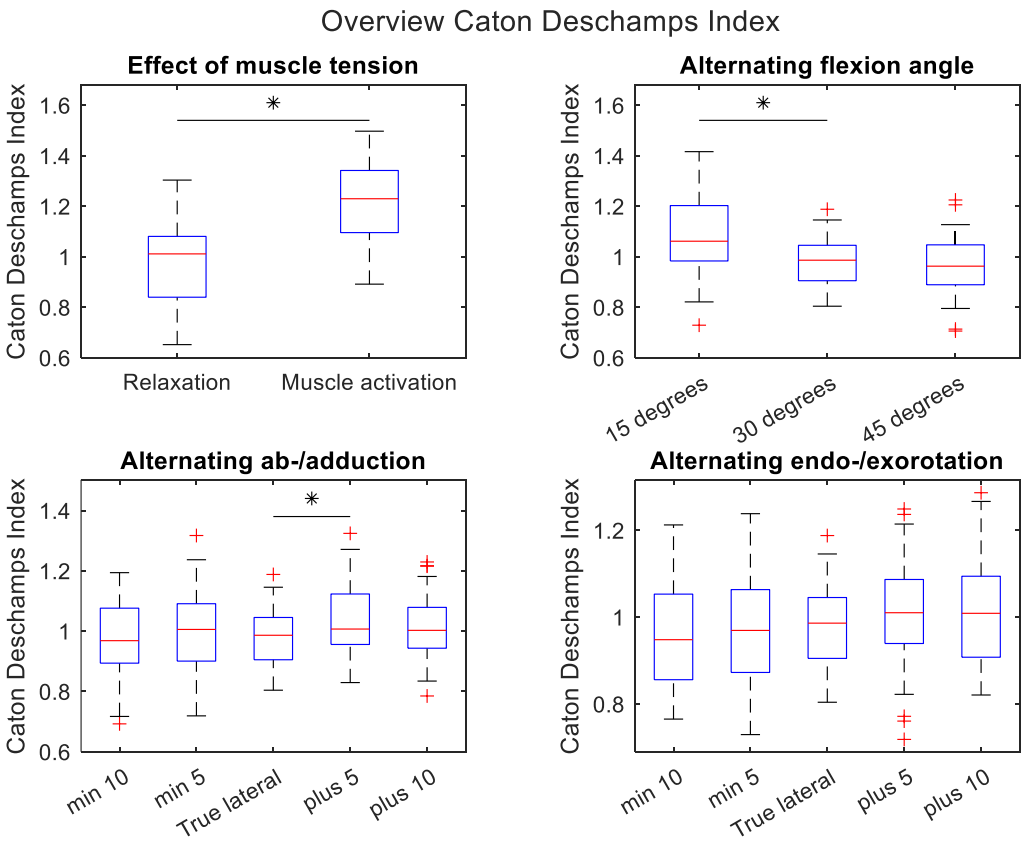

Figure 14. Overview of CDI, statistical differences are displayed with an asterisk (*).

Insall Salvati Index

For the ISI the boxplots of the four subgroups are visualized in Figure 15. The median of the static ISI is 1.01 (IQR 0.90 and 1.13) and the median of the dynamic ISI is 1.11 (IQR 0.97 and 1.25), resulting in a significantly higher ISI in the dynamic scan in relation to the static scan (p-value <0.001). In contrast with the CDI, changing the tibiofemoral angle does not influence the ISI. Besides this, all the alternations regarding the true lateral deviations were not statistically different.

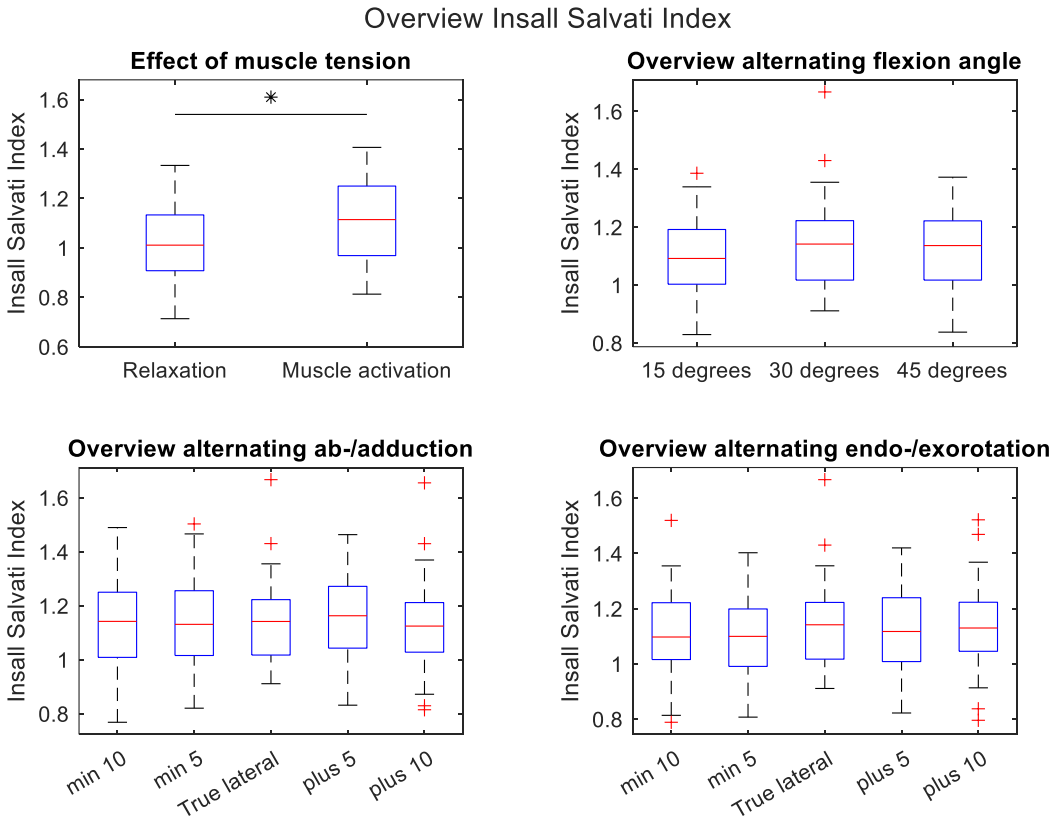

Figure 15. Overview of ISI, statistical differences are displayed with an asterisk (*).

One of the outliers that is visible in Figure 15, is the ISI of a true lateral projection with a tibiofemoral flexion angle of 30 degrees. The simulated X-ray with the selected points, used to calculate the ISI is visualized in Figure 16A and 16B. In comparison to these outliers, a simulated X-ray with the selected points (Figure 16C and 16D), of an average ISI is visualized.

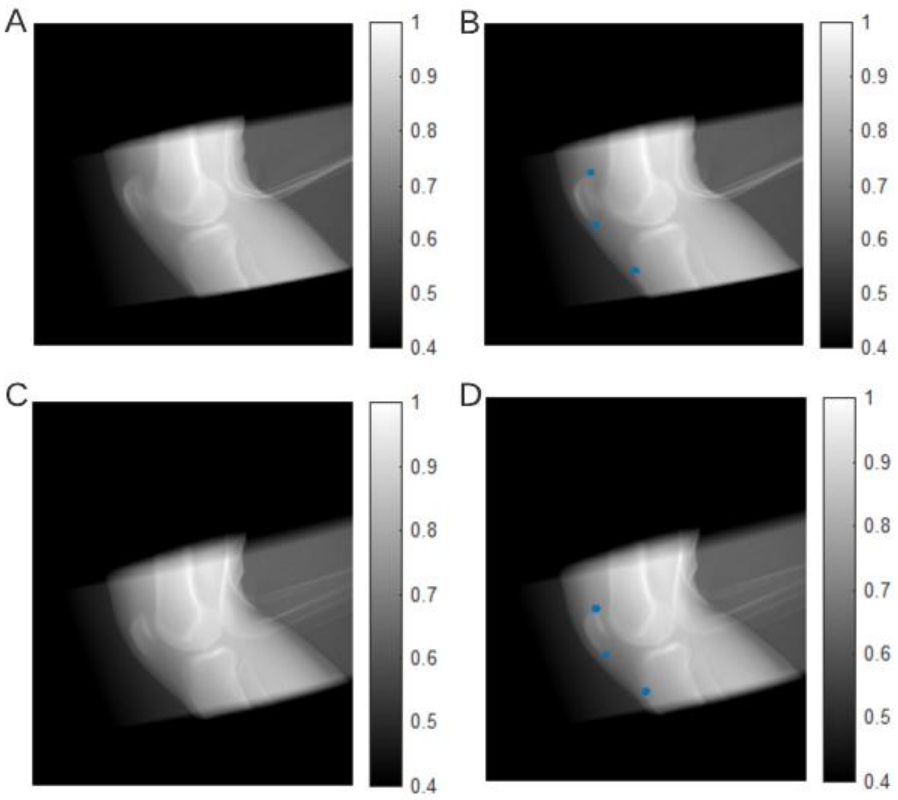

Figure 16. An example of an increased ISI. A. the simulated X-ray, with the outlier ISI, on which the point selection was performed. B. The same simulated X-ray as A with the selected blue points. C. the simulated X-ray, with the average ISI, on which the point selection was performed. D. The same simulated X-ray as C, with the selected blue points.

Discussion

The aim of this study was to assess the influence of position errors in flexion and extension, endo- and exorotation and ab- and adduction on the measured CDI and ISI for the assessment of patella alta. The main result was that a smaller tibiofemoral angle, 15° instead of 30°, results in an overestimation of the CDI. Secondly, this study shows that the ISI and CDI are insensitive for ab- and adduction and endo- and exorotation errors.

The study of Narkbunnam et al.[34] is currently the only research that investigated the effect of an alternating tibiofemoral angle using X-rays. In this research the effect of a tibiofemoral angle of 0°, 30°, and 60° on the measured patella height was investigated, and they found a significant difference for both the CDI and ISI. It was reported that this was not clinically relevant, because it fell within the SD range. Increasing the tibiofemoral angle from 0° to 30° showed the biggest difference, namely an increase of 0.071 for the ISI.[34]

Their findings are in contrast to the current study, in which only a smaller tibiofemoral angle in combination with the CDI was found to be statistically different. For this study a tibiofemoral angle of 15°, in comparison with 30°, resulted in an increase of 0.08 for the CDI. This small difference is expected to be clinically irrelevant, keeping in mind the wide normal range from 0.8-1.2 for the CDI.

Another research, of Becher et al. used MRI to assess the effect of knee flection on the CDI and ISI, they used similar tibiofemoral angles, namely 0°, 15°, 30° and 45°. In their research no statistical differences were found when changing this angle.

Only one previous study was found regarding the effect of ab-/adduction or endo-/exorotation on the CDI and ISI. The study, conducted by Huddleston et al.[30], which was performed using cadaver knees, showed an axial counterclockwise rotation of the C-arm revealed statistically significant differences for the CDI. However, when looking at the mean and range of the CDI these differences are very small. In contrast to this study, our research showed that only an adduction of 5° in combination with the CDI was found to be statistically different. An adduction of 5° resulted in an increase of the median of 0.0206. This small increase, in combination with the boxplot in Figure 5, suggests that these differences are expected to be within the margin of error.

Multiple studies described that activation of the quadriceps muscles increases the CDI and ISI significantly.[34,38] These previous studies used lateral X-rays in weight-bearing and non-weight bearing positions to reach this result. The use of these X-rays however, could result in variations other than the quadriceps muscle activation, such as endo-/exorotation and ab-/adduction, which could affect this outcome. This current research confirmed that these findings are most likely related to muscle activation.

However, in this current research it is uncertain whether the volunteers are completely relaxed during the static scan. The CDI showed a decrease with muscle activation for one volunteer, from 1.08 to 1.00. When looking at the ISI a decrease was present for 6 volunteers, with a difference ranging from 0.02 to 0.08. When the volunteers are not completely relaxed,

quadriceps activation will be present during the static scan, which will influence the measurements. Therefore, it is important that, when the lateral X-ray is made, patients are as relaxed as possible, to prevent an overestimation of both the CDI and ISI.

Limitations

One of the most important limitations was the quality of the created projections. These average intensity projections were of low resolution. This made it more difficult to select the corresponding points required to calculate the CDI and ISI. In this study, no repetitive measurements were conducted to determine the reproducibility of the point selection. In previous research[39], a good intra- and interobserver variability was found for both the CDI and ISI on conventional X-rays. The decrease in quality of these projections gives reasons to doubt these intra- and interobserver variability for this research. Therefore, further research should be conducted to determine the reproducibility using the projections in comparison to the conventional X-rays.

Another limitation is the deviation from the desired tibiofemoral angle of 15°, 30° and 45°. These deviations were on average below 1°, which will only influence the measurements slightly.

The margin of error is also influenced by the accuracy of the processing steps of the 4D CT data. The processing steps in this study were similar to a previous study of Chen et al.[35]. The only difference was automatic instead of manual bone segmentation, with a DICE of 0.99 for the femur, 0.98 for the tibia and 0.96 for the patella[27]. In the research of Chen et al. an average registration variability of approximately 0.6 mm was found, resulting in a small effect on the margin of error.

Conclusion

Overall, this research shows that both the CDI and ISI are robust measurements. Minor and clinically irrelevant changes were seen for the CDI when altering the flexion angle to 15° and when an adduction of 5° was present. Furthermore, this study confirms the effect of muscle activation on both the CDI and the ISI.

Chapter 3: A novel method for patellar lateralization

Introduction

Knowledge on patellofemoral kinematics is important to get more insight into patellar disarticulation. The chance of patellar disarticulation is increased with lateralization of the patella in comparison to the trochlear groove. Currently, this lateralization is determined using the tibial tuberosity-trochlear groove (TT-TG) distance or the mediolateral translation of the patella. The TT-TG distance is calculated, using the deepest part of the trochlear groove and the most prominent part of the tibial tubercle, this is visualized in Figure 17A.[40]

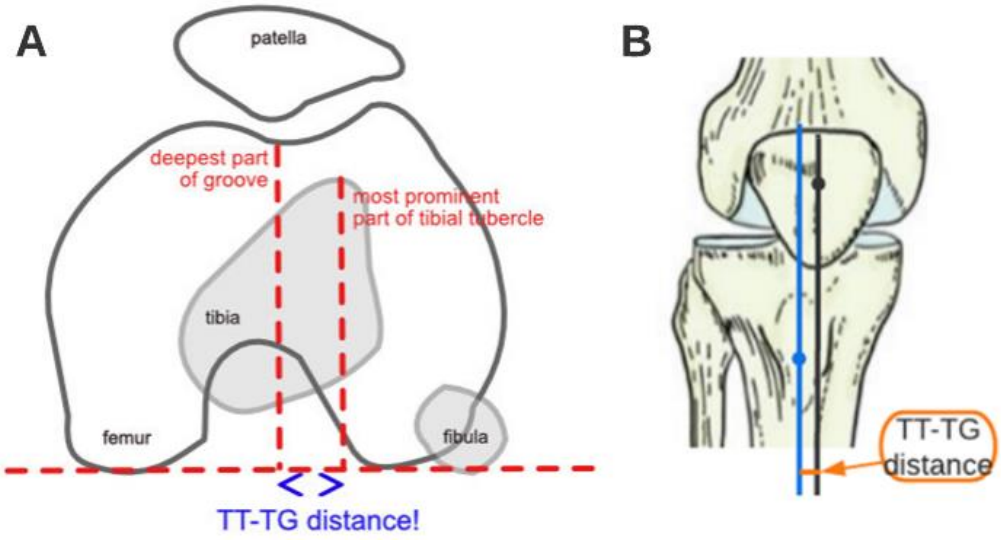

Figure 17. A. An axial projection of the knee in full extension, which is used for the calculation of the tibial tuberosity-trochlear groove (TT-TG) distance. B. Frontal view, with the distance between the trochlear groove (black dot) and tibial tuberosity (blue dot). [40]

Currently, axial slices of MRI or CT scans, with the knee in full extension, are used to measure the TT-TG distance.[41] It is reported that in patients with patellar instability the TT-TG distance is increased in 56% of the cases, in comparison to only 3.5% of healthy controls.[14] Currently, a TT-TG distance below 15 mm is assumed to be normal, and a distance above 20 mm is used as the cut-off value for an operation indication. An enlarged TT-TG distance is associated with an increased risk for patellar instability.

Besides, this measurement could be sensitive for incorrect positioning, and is based on a 2D measurement of only one distance. Therefore, a robust and elaborate measurement method, to obtain more information about the lateralization during flexion, could be of added value.

In previous research[42,43], the mediolateral translation of the patella was determined in the sagittal plane. These studies also showed that the lateral translation is increased in patients with patellar instability. This was especially evident in extension and during the first degrees of flexion, showing a maximum translation of 14 mm in extension. Flexion is determined to be a more stable situation, with minimal to no lateral translation.

To extend the knowledge of patellofemoral kinematics, it can be of added value to investigate the relationship between the lateral translation of the patella and the trochlear groove. Besides that, with the use of the 4D CT protocol, available at the Radboudumc Nijmegen, the motion of the knee bones (patella, femur, tibia) can also be addressed. With these opportunities a novel method to address patellar maltracking could be developed.

The purpose of this study was to create a novel method to determine patellar lateralization relative to the trochlear groove. This new method will be used to compare healthy volunteers with patients with patellofemoral instability. Within the patient population, a comparison will also be made between the affected and unaffected knee, to identify possible differences. In the end, this method may provide new insights into the anatomical variations regarding patellar instability and could potentially lead to improved methods for diagnosing and optimal treatment of this condition.

Methods

Data acquisition

For this research two different databases were used. First, the same database, as used in Chapter 2, of 100 healthy volunteers was used. In addition to this, a database consisting of static and dynamic CT scans of patients with patellofemoral instability was used. Both groups had undergone a conventional 3D CT scan and a 4D CT scan on a Canon Aquilion One Genesis scanner. At first the conventional 3D CT was made of both knees in full extension, Figure 17a. Then, the 4D CT scan was made, acquiring 41 scans during an active flexion-extension-flexion movement (90° of flexion to full extension) in roughly 10 seconds, (Figure 17b,c).

Figure 17. a) 3D or static CT, with knees fully extended; b) 4D or dynamic CT with the knees in 90° flexion; c) 4D or dynamic CT with the knees fully extended.[27]

To same steps were taken as in Chapter 2, to create the transformations from the static to the dynamic CT scan. Masks of the tibia, femur and patella were created to assess 3D surface meshes of the bone, determine the tibiofemoral angle and to calculate the transformations from the positions of the tibia, femur and patella in the conventional CT scans to the corresponding positions in the 4D CT scans.

Patient inclusion

Of the CT database of 100 healthy volunteers, a total of 198 knees from 99 participants were included in this study. One volunteer was excluded, because of a scanning error. This resulted in an insufficient visibility of the tibia, making it impossible to calculate the transformations.

A total of 42 knees from 21 patients with PFI were included initially. Patients with both unilateral and bilateral PFI were eligible for this study. All patients were treated by an orthopaedic surgeon at the Radboudumc.

Calculation of trochlear rollout

During previous unpublished research a primary set-up for this study had already been created. The first steps were taken based on a study conducted by Boruhkov et al.[44] who aimed to describe the native trochlear orientation. In these steps, the medial condyle, lateral condyle and trochlear groove were determined automatically using the static CT scan. To determine these three points, namely the medial condyle, lateral condyle and trochlear groove, coaxial cutting planes were used. In this research a total of 100 coaxial cutting planes (Figure 19A), divided between the start- and endpoint of the trochlear groove (Figure 18), were used, in contrast to the research of Boruhkov et al.[44] who only used 11 cutting planes.

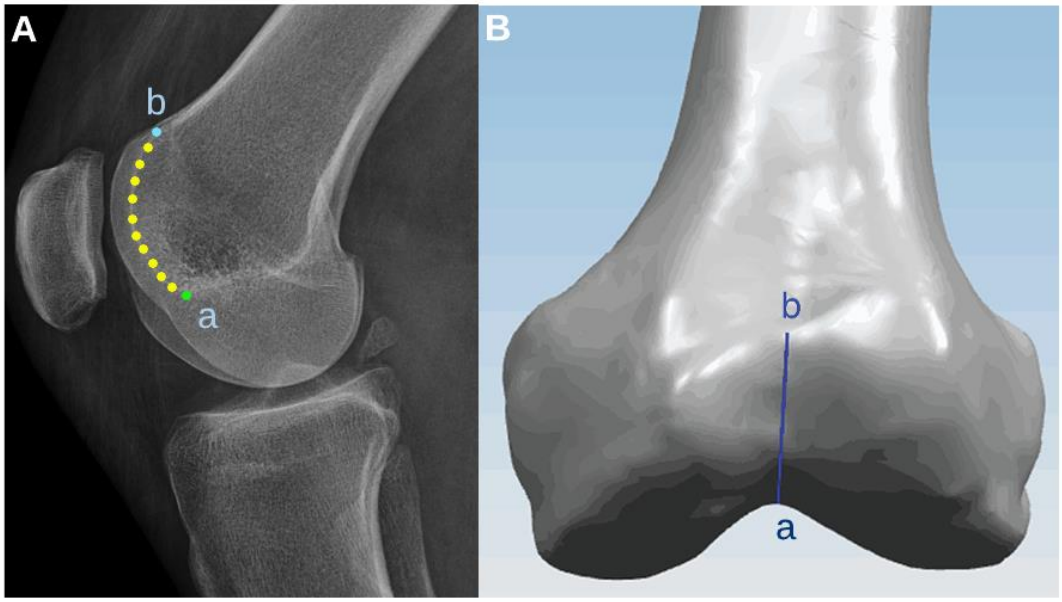

Figure 18. Visualization of the trochlear groove in two directions, there should be 100 yellow points, representing the 100 coaxial cutting planes. A. Visualization of the trochlear groove on a lateral X-ray. The blue dot represent the most proximal part of the groove and the 0% point. The green dot represents the notch and the 100% point. B. 3D visualization, b represents the proximal and 0% point, were the patella is located during extension, a represents the notch and 100% point, where the patella is located during flexion.[45,46].

These coaxial cutting planes were used to determine the peaks of the medial and lateral condyle. The condyles were determined using only the right part, in Figure 19A, of the plane using the edge points, of the convex hull, of this part of the plane. An example of this plane, with the determined condyle points, is visualized in Figure 19B. With the use of these condyles, the location of the trochlear groove was determined. The trochlear groove was determined to lay within the points of both condyles. Per condyle, lines were drawn through the condyle and the corresponding half of the possible points which could represent the trochlear groove. Per line, the distance from the line to all possible groove points was determined. The intersection of the lines, one for the medial condyle and one for the lateral condyle, with the smallest overall distance was determined to be the trochlear groove (Figure 19C).

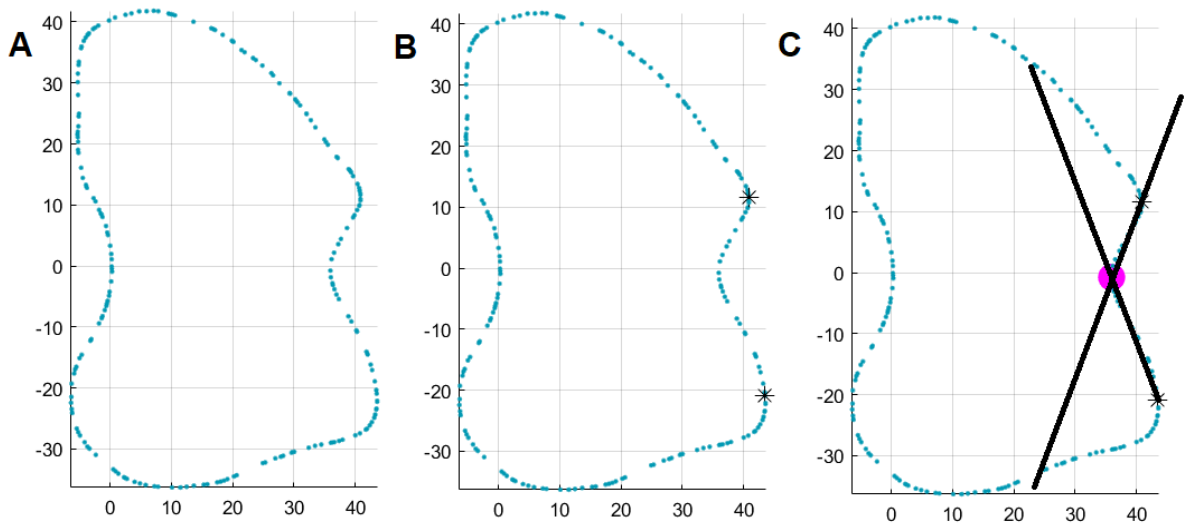

Figure 19. A. Visualization of the used coaxial cutting planes. B. the used coaxial cutting planes with the used condyles points shown in black. C. the used coaxial cutting planes with the best fitted lines (black) and the trochlear groove (magenta).

The next step was to add the patella, and its tracking pattern using the 4D CT scans. At first, the 4D CT data was linearly interpolated between the scanned tibiofemoral flexion angles, to obtain the transformations per degree of flexion. This will increase the number of transformations and subsequently increase the number of data points. To provide information of the whole movement, the following steps were conducted using the interpolated transformations. The first step was to determine the origin of both the patella and femur, this was done using the ERCKneeReferenceFrames[36]. For the patella, a center of mass determination was used, visualized as the green dot in Figure 20. For the femoral origin, two cylinders were drawn through both condyles. Next, a line was drawn through the center of these two cylinders. The origin of the femur was defined as the midpoint of this line, visualized as the purple dot in Figure 19. To determine the location of the patella, in relation to the trochlear groove a line was drawn from the origin of the patella to the origin of the femur. The cross sectional-point of this line with the femoral mesh, further mentioned as patellar projection point, was determined to be the location of the patella in relation to the trochlear groove; this is visualized in Figure 19. To find the location of the patellar projection point in relation to the trochlear groove, the closest coaxial cutting plane was determined. This was used later on to combine the data of all healthy volunteers as well as the data of all patients.

Figure 20. Overview of the method used to determine patellar projection point. Red: patella, green: patellar origin, blue: femur, purple: femoral origin, cyan: line from origin patella to origin femur, black: patellar projection point.

It was important to adjust this cross-sectional point to the same world coordinate system as the trochlear groove. With the use of the ERCKneeReferenceFrames, the transformation from the scanner coordinate system to the world coordinate system was calculated. With the use of this transformation and the previously calculated transformations from the static to the dynamic CT scan, the cross-sectional point was transformed to the static world coordinate system. Subsequently, the mediolateral translation in the frontal plane was determined and used for the 2D visualization. Patients with PFI could have a smaller lateral condyle, which will influence the mediolateral translation of the groove in relation to the origin of the femur. To correct for this, femoral translation were calculated relative to the femoral notch, the 100% point. The mediolateral translations of all knees were visually checked to exclude knees in which the trochlear groove could not be determined correctly. This was measured as sudden jumps in location of > 5 mm or a total mediolateral shift of > 10 mm. When the 2D data showed an aberrant movement throughout the whole groove (Figure 21), this knee was excluded from the database. When only a small part of the groove deemed inaccurate it was determined to change these parts to a NaN value, leaving them out of the analysis. When the 2D visualization was inconclusive, 3D visualization of the trochlear groove in comparison to the CT data was used to make a final decision.

For the healthy volunteers, a total of 2 right knees did not pass the quality checks and were excluded. Besides the exclusions, data of 6 knees was manually adjusted to correct for incorrect groove alignment in the proximal part of the groove.

In the PFI group a total of 4 knees, 1 right and 3 left, did not pass the quality checks and were excluded. Data was manually adjusted for 6 knees, as a correction for the incorrect alignment of the trochlear groove.

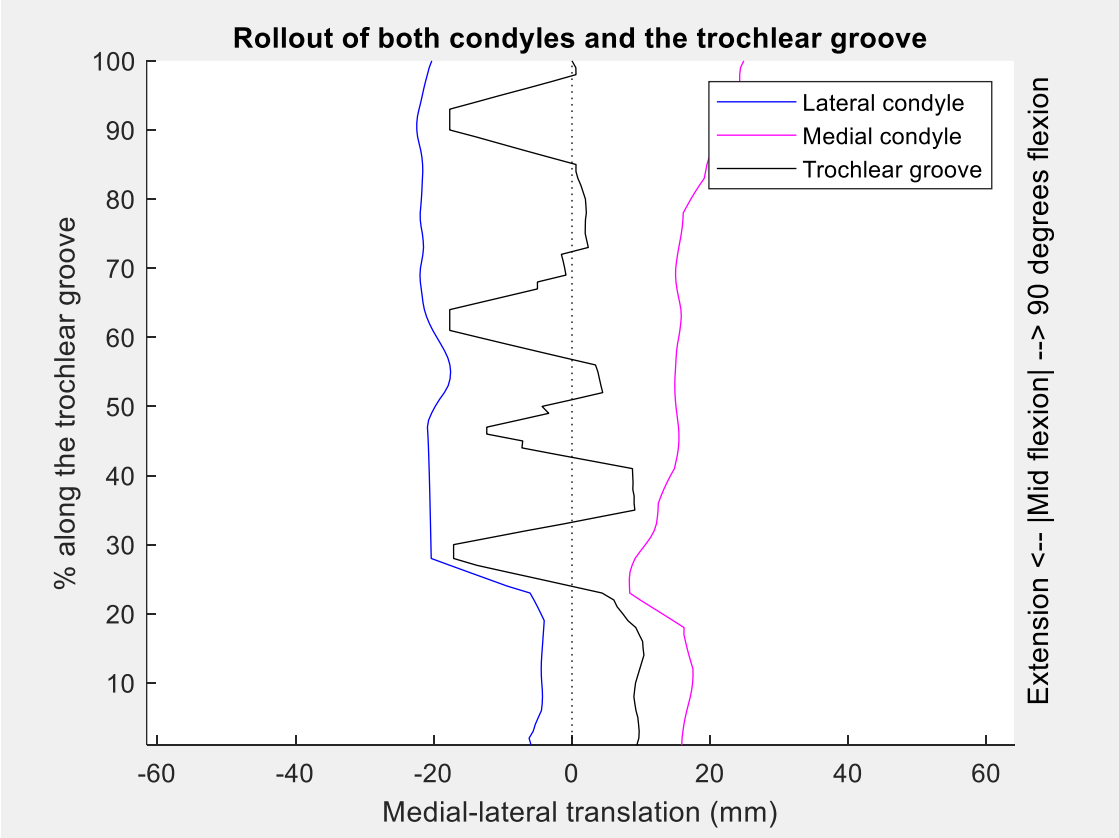

Figure 21. An example of an excluded knee due to an incorrect determination of the trochlear groove.

To quantify this measurement method, the distance between the patellar projection point and the trochlear groove was calculated. An overview of all steps conducted is provided in Figure 22.

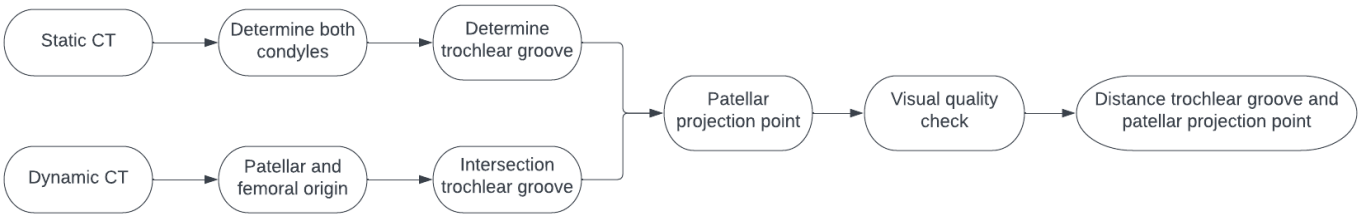

Figure 22. Flowchart of the steps conducted to determine the distance between the trochlear groove and the patellar projection point.

Data analysis

To further analyze the lateral-medial translation in patients with PFI, a comparison was made between the healthy volunteers and the patient group. Besides this, the patient population was also divided into two subgroups. Subgroup one consisted of the affected knees of the PFI patients and subgroup two consisted of the unaffected knees. These subgroups were chosen to first compare the affected and unaffected knees. When these were similar, all data could be used for the comparison with the healthy volunteers.

To visually compare the results of the different subgroups, the mean and standard deviation of the mediolateral translation was calculated per coaxial cutting plane and displayed in a 2D plot.

Besides that, the distance between the patellar projection points and the trochlear groove was calculated and analyzed. The first step was to determine if the data of this distance was distributed normally. This was done using the Kolmogorov-Smirnov test. When this test revealed that the data was not distributed normally a visual check of the histograms was conducted. In the end it was accepted that all data was distributed normally, because based on the Kolmogorov-Smirnov test only a small percentage was indicated as not a normal distribution and these histograms looked sufficient.

An independent t-test was used to determine if any significant differences were present. Due to the high number of t-tests that were performed, a p-value below 0.001 was used as statistically different.

Results

The final population of healthy volunteers consists of 196 knees of 99 participants, 29 men and 70 women with a mean age of 24.2 years. The PFI population consists of 38 knees from 21 patients, 8 men and 13 women with a mean age of 22.2 years. More elaborate patient characteristics can be found in table 2.

Table 2. Patient characteristics

	Healthy volunteers (n = 99)	PFI patients (n = 21)
Age (year)	24.2 (range 18-34)	22.2 (range 15-33)
Gender (f/m)	70/29	13/8
Weight (kg)	68.0 (range 51-98)	75.3 (range 54-141)
Height (cm)	174.1 (range 158-198)	175.9 (range 155-190)
Affected knee		
Unilateral	n/a	18
Bilateral	n/a	3

Healthy volunteers

An example of the trochlear rollout of one healthy volunteer is visualized in Figure 23A. An overview of the mean trochlear rollout of the healthy volunteers is visualized in Figure 23B. On average, the trochlear groove translated with maximally 1 mm in medial direction (SD, 4 mm), and did not show any lateral translation (SD, 3.5 mm). The patellar projection point showed a mean medial translation of 1 mm (SD, 2 mm), and a mean lateral translation of 1 mm (SD, 3.5 mm). Besides this, it is visible that the standard deviation range of the patellar projection point is almost entirely located within the range of the trochlear groove.

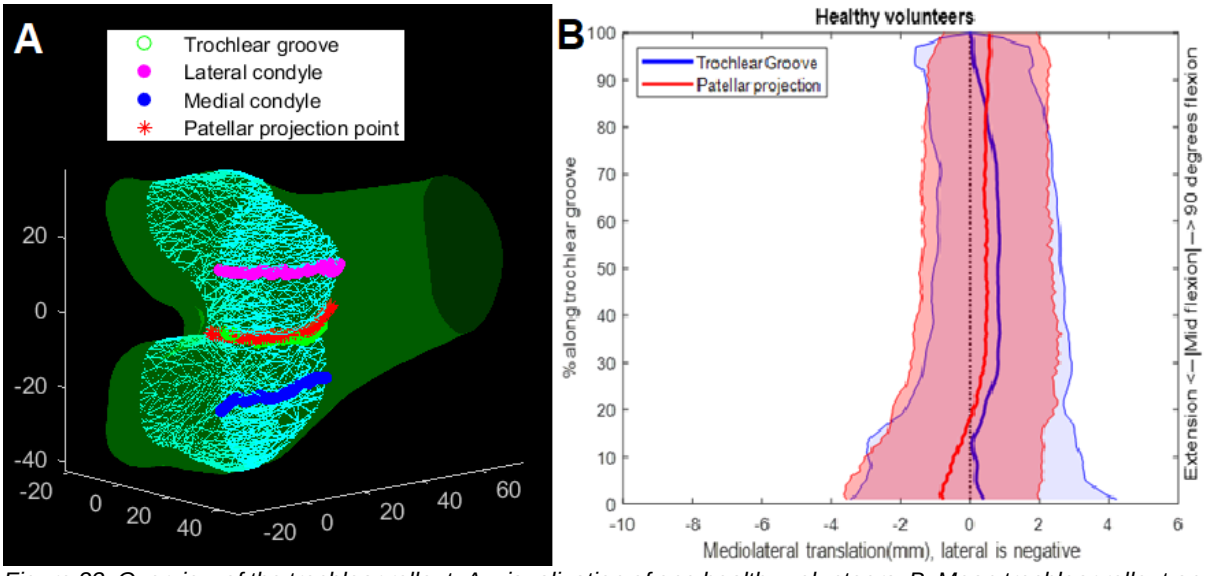

Figure 23. Overview of the trochlear rollout. A. visualization of one healthy volunteers. B. Mean trochlear rollout and its standard deviation, of healthy volunteers. The dotted line represents the notch, the zero point of the x-axis.

Patients with patellofemoral instability

Data of the affected and unaffected knees was subdivided (Figure 24). The trochlear groove showed a mean medial translation of 1 mm (SD, 4 mm), and a mean lateral translation of 0.5 mm (SD, 3.5 mm). For the patellar projection point, the mean translation varies between 0.5 and 5 mm lateral translation, with a standard deviation range from 2 mm medial to 10 mm lateral translation. The patellar point is more lateral translated in the proximal part of the trochlear groove, when the knee is in extension. When looking at the distal part of the trochlear groove and when the knee is in deep flexion, the lateral translation of the patellar projection point is limited, but still visible. Besides that, the shape of both the trochlear groove and the patellar projection point is similar for both subgroups. The independent t-test, used for the comparison between the affected and unaffected knees of the patients with PFI, showed no significant differences throughout the entire trochlear groove.

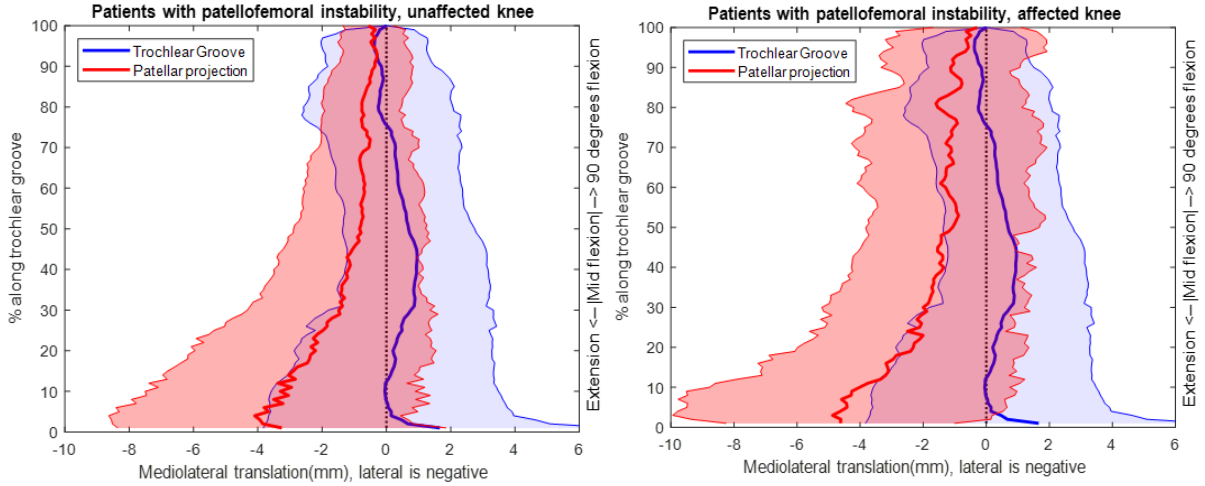

Figure 24. Overview of the mean trochlear rollout, and its standard deviation, of patients with PFI, left the unaffected knees, and right the affected knees.

Two individual patients with PFI were selected to visualize the differences on patient level. The rollout of the affected left knee of one patient, Figure 25, showed lateralization of the patellar projection point through the whole trochlear groove. For this patient the measured TT-TG distance was 15.4 mm. In contrast to the lateralization of the patellar projection points, also normal tracking patterns were present in the patient population. Figure 26 shows the rollout of the affected left knee of one patient, for this patient a TT-TG distance of 19.9 mm was measured. A normal tracking pattern can be seen throughout the whole trochlear groove.

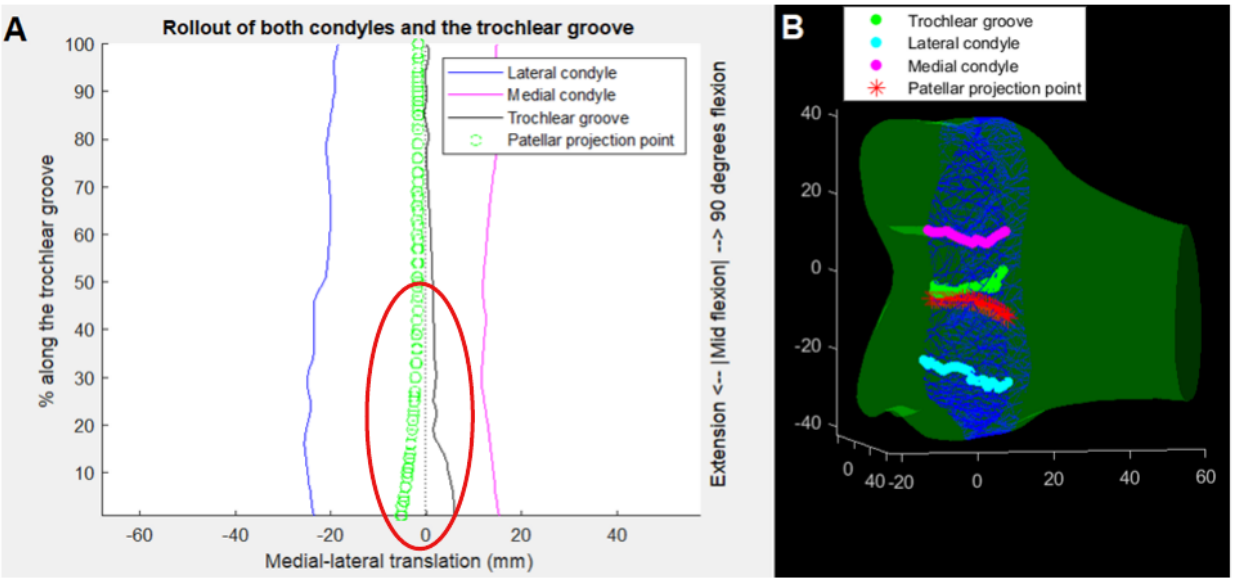

Figure 25. Visualization of an individual patient. A. 2D visualization of the condyles, trochlear groove and the patellar projection point. B. 3D visualization it can be seen that the lateralization is most prominent in the proximal part of the trochlear groove during extension (red ellipse).

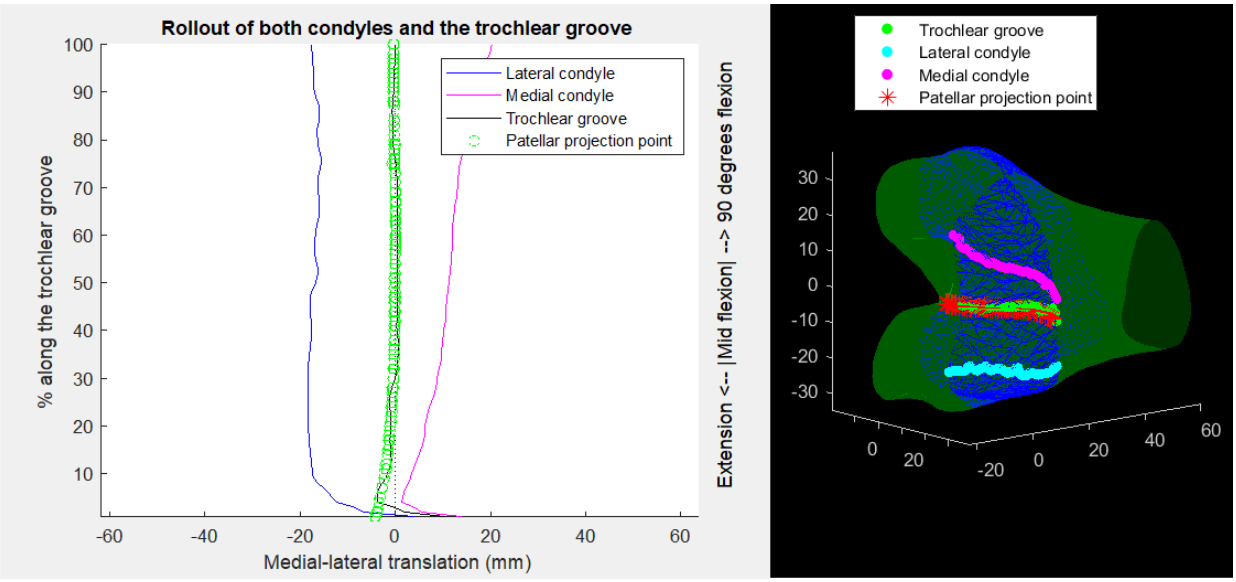

Figure 26. Visualization of another individual patient, with a normal tracking pattern.

Healthy volunteers vs patients with PFI

When comparing the distance between the patellar projection point and the trochlear groove, between healthy volunteers and patients with PFI, this distance is significantly increased in some parts of the trochlear groove (Figure 27). An overview of the significantly different parts of the trochlear groove can be found in Table 3.

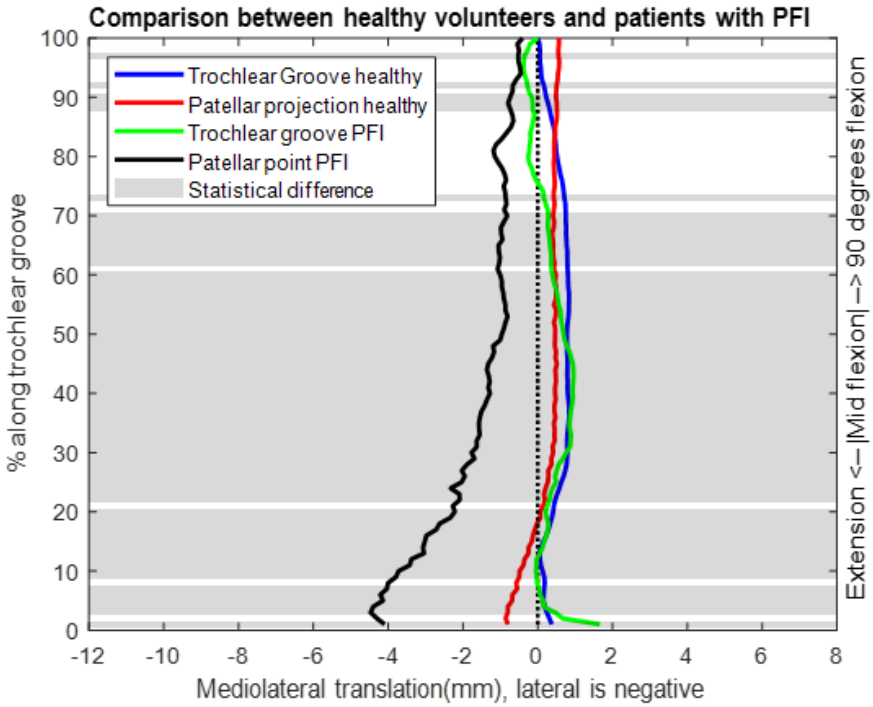

Figure 27. Comparison of the distance between the patellar projection point and the trochlear groove between patients with PFI and healthy volunteers. The shaded areas indicate a statistically significant difference.

Table 3. Overview of the significant different parts of the trochlear groove for the distance between the patellar projection point and the trochlear groove.

	Healthy vs all PFI	Healthy vs Unaffected	Healthy vs Affected	Affected vs unaffected
Trochlea-patella distance	1, 3-7, 9-20, 22-60, 62-70, 73, 88-90, 92, 97	1, 2-5, 7, 9, 12, 14, 16, 18, 20, 22-70, 74, 75, 88, 97	1, 3, 6, 7, 9-11, 14-17, 19, 20, 22, 23, 25, 26, 29-38, 39-52, 54, 56, 57, 73, 88, 90, 91	none

Discussion

The aim of this study was to develop a novel method to represent the mediolateral translation of the patella in relation to the trochlear groove during an active flexion-extension-flexion movement. With this novel method a comparison was made between patients with PFI and healthy volunteers. This novel method revealed a lateralization of the patella in relation to the trochlear groove, mostly during extension and a small tibiofemoral flexion angle. It also showed a persistent lateralization during 90° flexion in the condylar notch.

When comparing to previous research, two different studies were found which used dynamic imaging to assess the patellar maltracking. The study of Tanaka et al.[47] used a similar scanning protocol to obtain dynamic CT scans. In contrast to this research, they only used 10 slices

ranging from 0 to 90°, with an interval of 10° for the analysis. They used an different method to determine the amount of lateralization, namely the bisect offset measurement. Which showed four different tracking patterns among the population, namely: normal tracking, lateral tracking, j-sign pattern and reversed j-sign pattern. The j-sign pattern was present in 78% of the knees. This is similar to this research, when looking at the mean of the patellar projection point in patients with PFI. No comparison was made between patients and healthy volunteers, making it not possible to compare these results.[47]

The study by Frings et al.[48] used dynamic magnetic resonance imaging (MRI), with a range of motion from 0 to 40°. The mediolateral translation of the patella was manually determined, using only two transversely oriented frames, namely 30° of flexion and extension. They also described an increased lateral translation in patients in comparison to healthy controls.[48]

A significant difference was found for the distance between the patellar projection point and the trochlear groove for the first half of the trochlear groove. However, when looking at the individual patient, Figure 26, a normal tracking pattern was visualized. This was in contrast with what was expected, based on the increased TT-TG distance and the patients complaints. This confirms the fact that not all patients need to have all predisposing factors. When looking at the lateral tracking in Figure 25, the TT-TG distance, 15.4 mm, is smaller than expected. This could be explained due to the medial location of the trochlear groove, because a medial trochlear groove will decrease the TT-TG distance. This will also increase the distance between the patellar projection point and the trochlear groove, resulting in a more lateral tracking pattern. Another factor that influences the TT-TG distance is the rotation of the tibia. When the tibia is exorotated, the tibial tuberosity is located more laterally, resulting in an increased TT-TG distance. These variabilities raises questions if the TT-TG distance is comparable to this novel method. It is expected that this novel method could replace the TT-TG distance once further developed.

Determination of the trochlear groove was based on the research of Boruhkov et al.[44]. They described a small lateral translation of the trochlear groove, which was most prominent in the middle of the trochlear groove. This was in contrast with the current research, in which a small medial translation was visible. Besides this difference, similar distances in translation were visible between both studies.

During flexion, lateralization of the patella was visible in the notch of the trochlear groove in patients with PFI. This was unexpected since patellar luxation occurs most often during the first 30° of flexion.[49] Besides that, it is believed that trochlear dysplasia is less pronounced or absent in the distal part of the trochlear groove.[15] This lateralization could be explained due to a different shape of the patella, for example Wiberg classification III, which is more often present in patients with PFI.[50] With a Wiberg type III patella, the center of mass or origin is located more laterally than the deepest point of the patella. Therefore, the use of this method could overestimate the lateral translation of the patella in patients with a Wiberg type III classification of the patella.

In extension, when the patella is at the proximal part of the groove, the lateralization is most prominent. This can be explained due to multiple anatomical variations, which could be present in patients with PFI. This is mostly affected by the trochlear dysplasia which is more pronounced at the proximal part of the groove.[15] During active extension, the activation of the quadriceps muscle pulls the patella laterally. This quadriceps pulling force is affected by the q-angle, which is increased with a lateralized tibial tubercle.[51] In healthy volunteers, this lateralization is prevented by the lateral condyle. In patients with PFI this condyle is smaller, and the trochlear groove is shallower, resulting in a smaller lateral barrier.

Limitations

The smaller size of the lateral condyle can influence the results. The calculation of the origin of the distal femur is based on the center of the condyles. When the lateral condyle is smaller

the origin is located more medially in comparison to the trochlear groove. When this origin is used as a starting point for the mediolateral translation, the distance between the patellar projection point and the trochlear groove will remain the same, but the orientation of the groove will be lateralized incorrectly.

The combination of this novel method and a severe trochlear dysplasia is currently not possible. When there is a severe trochlear dysplasia the algorithm is not able to correctly identify both condyles and the trochlear groove. Sometimes, the trochlear groove is completely absent and cannot be identified. When a very shallow groove is present, this method cannot be applied as well. Due to an incorrect determination 9.5% of the knees of patients with PFI needed to be excluded in comparison to 1% of the healthy knees.

When looking at the determination of the starting point of the trochlear groove, some improvements are required to optimize this method. When looking at the patient population, for example Figure 26, it can be seen that the determination of the first part of the groove was incorrect. In patients with PFI the trochlear groove is often shorter than in the healthy population, this could explain this wrong determination, because the algorithm was written for healthy volunteers. Besides, it can be questioned if the current method to determine the trochlear groove is the most optimal. Other methods, for example a method based on the bony landmarks, which are also present in patients with severe dysplasia, should be looked at.

The sample size of the patients with PFI were relatively small, as small as 17 knees for the non-affected knees group. Because of this, it is possible that the outcomes are not representable for the whole patient population. Besides this the data could be biased due to some extreme observations. This is taken into account by the visual check of all individual 2D visualizations. Besides that, the sample size was already bigger in comparison to the research of Frings et al.[48], who had a patient population of only 10 patients.

As mentioned before, only the center of mass of the patella was used to determine the patellar projection point. This could not represent the deepest point of the patella, which could result in a wrong determination of the distance between the patellar projection point and the trochlear groove. To obtain a broader picture of the relation between the patellar projection point and the trochlear groove, it would be of added value to include other points in the patella.

Conclusion

This research shows that this novel method showed similar results regarding patellar lateralization as expected. Lateralization throughout the whole trochlear groove, and during the whole flexion-extension-flexion movement, can be visualized and analyzed. A significant difference was present in lateralization between healthy volunteers and patients with PFI, mostly during the first part of the trochlear groove. No significant differences were found between the affected and unaffected knees of patients. To further optimize this novel method, the location of the origin of the patella should be optimized to correct for other patellas with different shapes, for example the Wiberg III classification.

Conclusion and further research

The aim of this thesis was to increase the knowledge regarding the effect of the predisposing factors for patellar instability and luxations.

Based on Chapter II it can be concluded that both measurement methods, the Caton-Deschamps index and the Insall-Salvati index, are robust methods to evaluate patella alta on an X-ray. This research also showed an increased indices with muscle tension for both methods. Therefore, it is important that, X-rays without muscle tension are used to determine the presence of patella alta, when using the current cut-off values. Further research should focus on determining the reproducibility using the projections in comparison to the conventional X-rays. Besides that, the coherence of the calculated indices should be evaluated between CT and a conventional X-ray.

Chapter III revealed a promising starting point for a new method to quantify and visualize the relationship between the patellar projection point and the trochlear groove during motion. With this method patellar lateralization was shown for the average patient with patellofemoral instability was confirmed. This method can be further developed using multiple patella points to create a broader view of the patellar tracking. For example, the deepest point of the patella could be added, this point should normally follow the deepest point of the trochlear groove. Therefore, tracking this point could provide more clinically relevant information than the mid-point about the tracking pattern. It can also be extended by adding other patellar motions, such as the patellar tilt[52].

Improvements can also be made regarding the definition of the trochlear groove. The current method to determine the trochlear groove is sensitive to errors, particularly for dysplastic trochleae, which made the visual check essential. The distance between the patellar projection points and other points in the trochlear groove, for example midway between the condyle and trochlear groove can also provide extra information[47]. This information could be used to determine the part of the patella that is located within the range of the condyles for both healthy volunteers and patients with PFI.

With the large database of healthy volunteers that was created, the individual patients with PFI could be compared to this standard. This will provide the opportunity to apply this increased knowledge in individual patients. However, it needs to be kept in mind that the patient population is relatively diverse. Predisposing factors do vary among the population and not all factors are presents in each patient in a similar fashion.[53] When looking at the trochlear rollout, the patient that was selected in the Result section with an increased TT-TG distance did show a normal tracking pattern. This suggests that the method introduced in this research provides different outcomes than the standard TT-TG method used in clinical practise. Further research regarding the correlation between both measurement methods should be considered to optimize the clinical value of this new method. Furthermore, this method was based on a relative easy movement, flexion against gravity, during which the essence of the patellofemoral complaints may not be fully captured. Therefore, it could be of added value to expand the scanning protocol with more challenging movements and loads replicating activities of daily living that may be associated with complaints (e.g. walking, squatting, or pivoting on the foot)[54].

Finally, the possible opportunities using the 4D CT should be evaluated and extended. With this research only two of the possibly present predisposing factors were looked at. And only one of them, namely the patellar lateralization was used for a comparison between the patients with PFI and the healthy volunteers. Further research could focus on understanding the results of this novel method in comparison to the patients complaints. Furthermore, these results could be combined with other assessments of the patients to obtain a more holistic view of the pathology. This could focus on the effects of the predisposing factors, patella alta, trochlear dysplasia, increased TT-TG distance and an increased Q-angle in relation to each other. When all factors are taken into account it may become possible to develop an algorithm to further optimize the diagnostics and predict the effects of treatment per individual patient.

References

1. Smith MK, Werner BC, Diduch DR. Avoiding Complications with MPFL Reconstruction. *Curr Rev Musculoskelet Med*. 2018;11(2):241-252. doi:10.1007/S12178-018-9479-Y/TABLES/1

2. McCrum E, Cooper K, Wittstein J, French RJ. Imaging of Patellofemoral Instability. *Clin Sports Med*. 2021;40(4):693-712. doi:10.1016/J.CSM.2021.05.007

3. Hess RW. Knee MPFL Reconstruction FAQ.

4. Castelli A, Jannelli E, Calderoni EF, et al. MPFL reconstruction and tibial tuberosity transposition in patients with patellar instability: May it troubleshots also trochlear dysplasia? *J Exp Orthop*. 2021;8(1):1-10. doi:10.1186/S40634-021-00392-5/TABLES/5

5. Dislocated kneecap | informedhealth.org. Accessed May 5, 2023. https://www.informedhealth.org/dislocated-kneecap.html

6. Twomey KD, Fornari ED, Kirschner N, Sever R, Hanstein R. Risk factors for recurrent patellar instability in children and adolescents. *Pediatrics*. 2019;144(2_MeetingAbstract):764-764. doi:10.1542/PEDS.144.2MA8.764

7. Geenen E, Molenaers G, Martens M. Patella alta in patellofemoral instability. *Acta Orthop Belg*. 1989;55(3):387-393.

8. Leone E, Davenport S, Robertson C, et al. Incidence and risk factors for patellofemoral dislocation in adults with Charcot-Marie-Tooth disease: An observational study. *Physiother Res Int*. Published online 2023:e1996. doi:10.1002/PRI.1996

9. Wolfe S, Varacallo M, Thomas JD, Carroll JJ, Kahwaji CI. Patellar Instability. *StatPearls*. Published online February 19, 2023. Accessed April 14, 2023. https://www.ncbi.nlm.nih.gov/books/NBK482427/

10. Lenhart RL, Brandon SCE, Smith CR, Novacheck TF, Schwartz MH, Thelen DG. Influence of patellar position on the knee extensor mechanism in normal and crouched walking $. Published online 2016. doi:10.1016/j.jbiomech.2016.11.052

11. Kazley JM, Banerjee S. Classifications in Brief: The Dejour Classification of Trochlear Dysplasia. *Clin Orthop Relat Res*. 2019;477(10):2380. doi:10.1097/CORR.0000000000000886

12. Dong C, Zhao C, Li M, et al. Accuracy of tibial tuberosity-trochlear groove distance and tibial tuberosity-posterior cruciate ligament distance in terms of the severity of trochlear dysplasia. *J Orthop Surg Res*. 2021;16(1). doi:10.1186/S13018-021-02527-X

13. Cilengir AH, Dursun S, Sinci KA, Tosun O. Total Diz Artroplastisinin Preoperatif Radyolojik Değerlendirmesi. *Forbes Tıp Derg*. 2021;2(2):67-73. doi:10.5222/FORBES.2021.35119

14. Dejour H, Walch G, Nove-Josserand L, Guier C. Factors of patellar instability: an anatomic radiographic study. *Knee Surg Sports Traumatol Arthrosc*. 1994;2(1):19-26. doi:10.1007/BF01552649

15. Hao K, Niu Y, Kong L, Wang F. The patient with patellar instability has a stenotic intercondylar notch and a thin anterior cruciate ligament: a retrospective comparative study. *J Orthop Surg Res*. 2023;18(1):1-11. doi:10.1186/S13018-023-03632-9/TABLES/5

16. News. Accessed May 5, 2023. https://www.vbjs.com.au/news

17. Skouras AZ, Kanellopoulos AK, Stasi S, et al. Clinical Significance of the Static and Dynamic Q-angle. *Cureus*. 2022;14(5). doi:10.7759/CUREUS.24911

18. Mizuno Y, Kumagai M, Mattessich SM, et al. Q-angle influences tibiofemoral and patellofemoral kinematics. *J Orthop Res*. 2001;19(5):834-840. doi:10.1016/S0736-0266(01)00008-0

19. Patellofemoral Disorders | OrthoPaedia. Accessed April 23, 2023. https://orthopaedia.com/page/Patellofemoral-disorders

20. Ormeci T, Turkten I, Sakul BU. Radiological evaluation of patellofemoral instability and possible causes of assessment errors. *World J Methodol*. 2022;12(2):64. doi:10.5662/WJM.V12.I2.64

21. Dall'oca C, Elena N, Lunardelli E, Ulgelmo M, Magnan B. MPFL reconstruction: indications and results. *Acta Bio Medica Atenei Parm*. 2020;91(4-S):128. doi:10.23750/ABM.V91I4-S.9669

22. Colvin AC, West R V. Patellar instability. *J Bone Jt Surg*. 2008;90(12):2751-2762. doi:10.2106/JBJS.H.00211

23. Enea D, Canè PP, Fravisini M, Gigante A, Dei Giudici L. Distalization and Medialization of Tibial Tuberosity for the Treatment of Potential Patellar Instability with Patella Alta. *Joints*. 2018;6(2):80. doi:10.1055/S-0038-1661340

24. Bollier M, Fulkerson JP. The Role of Trochlear Dysplasia in Patellofemoral Instability. *JAAOS - J Am Acad Orthop Surg*. 2011;19(1). https://journals.lww.com/jaaos/Fulltext/2011/01000/The_Role_of_Trochlear_Dysplasia_in_Patellofemoral.2.aspx

25. Nolan JE, Schottel PC, Endres NK. Trochleoplasty: Indications and Technique. *Curr Rev Musculoskelet Med*. 2018;11(2):231. doi:10.1007/S12178-018-9478-Z

26. Dejour D, Saggin P. The sulcus deepening trochleoplasty-the Lyon's procedure. *Int Orthop*. 2010;34(2 SPECIAL ISSUE):311-316. doi:10.1007/S00264-009-0933-8

27. Dunning H, van de Groes SAW, Buckens CF, Prokop M, Verdonschot N, Janssen D. Fully automatic extraction of knee kinematics from dynamic CT imaging; normative tibiofemoral and patellofemoral kinematics of 100 healthy volunteers. *Knee*. 2023;41:9-17. doi:10.1016/J.KNEE.2022.12.011

28. Caton JH, Dejour D. Tibial tubercle osteotomy in patello-femoral instability and in patellar height abnormality. *Int Orthop*. 2010;34(2 SPECIAL ISSUE):305-309. doi:10.1007/S00264-009-0929-4/METRICS

29. Raja BS. Incidence of Patella Alta in Anterior Knee Pain- Assessment with Patellar Height Ratio's. *Orthop Sport Med Open Access J*. 2018;1(1). doi:10.32474/OSMOAJ.2018.01.000105

30. Huddleston HP, Redondo ML, Cregar WM, Christian DR, Hannon CP, Yanke AB. The Effect of Aberrant Rotation on Radiographic Patellar Height Measurement Using Canton-Deschamps Index: A Cadaveric Analysis. *J Knee Surg*. Published online 2021:254-260. doi:10.1055/S-0041-1731720/ID/JR200550OA-18

31. Phillips CL, Silver DAT, Schranz PJ, Mandalia V. The measurement of patellar height: A review of the methods of imaging. *J Bone Jt Surg - Ser B*. 2010;92(8):1045-1053. doi:10.1302/0301-620X.92B8.23794

32. Saffarini M, Alves P, Billieres J, Martin R. Medial UKA tends to increase patellar height, whereas open-wedge HTO tends to decrease patellar height. *Med Res Arch*.

2020;8(9). doi:10.18103/MRA.V8I9.2223

33. Patellar Height Measurement – Insall Salvati, Blackburne-Peel and Caton-Deschamps Indices | Bone and Spine. Accessed April 14, 2023. https://boneandspine.com/patellar-height-measurement/

34. Narkbunnam R, Chareancholvanich K. Effect of patient position on measurement of patellar height ratio. *Arch Orthop Trauma Surg*. 2015;135(8):1151-1156. doi:10.1007/S00402-015-2268-9/METRICS

35. Chen H, Kluijtmans L, Bakker M, et al. A robust and semi-automatic quantitative measurement of patellofemoral instability based on four dimensional computed tomography. *Med Eng Phys*. 2020;78:29-38. doi:10.1016/J.MEDENGPHY.2020.01.012

36. Miranda DL, Rainbow MJ, Leventhal EL, Crisco JJ, Fleming BC. Automatic determination of anatomical coordinate systems for three-dimensional bone models of the isolated human knee. *J Biomech*. 2010;43(8):1623-1626. doi:10.1016/J.JBIOMECH.2010.01.036

37. Wang S, Xiao Z, Lu Y, Zhang Z, Lv F. Radiographic Optimization of The Lateral Position of The Knee Joint Aided by CT Images and The Maximum Intensity Projection Technique. Published online 2021. doi:10.21203/rs.3.rs-744837/v1

38. Yiannakopoulos CK, Mataragas E, Antonogiannakis E. The effect of quadriceps contraction during weight-bearing on four patellar height indices. *J Bone Joint Surg Br*. 2008;90(7):871-873. doi:10.1302/0301-620X.90B7.20111

39. Verhulst F V., van Sambeeck JDP, Olthuis GS, van der Ree J, Koëter S. Patellar height measurements: Insall-Salvati ratio is most reliable method. *Knee Surg Sports Traumatol Arthrosc*. 2020;28(3):869-875. doi:10.1007/S00167-019-05531-1

40. TT-TG distance | KNEEguru. Accessed April 14, 2023. https://www.kneeguru.co.uk/KNEEnotes/articles/expert-views/2017/tt-tg-distance

41. Camp CL, Stuart MJ, Krych AJ, et al. CT and MRI measurements of tibial tubercle-trochlear groove distances are not equivalent in patients with patellar instability. *Am J Sports Med*. 2013;41(8):1835-1840. doi:10.1177/0363546513484895

42. Cregar WM, Huddleston HP, Shewman EF, Cole BJ, Yanke AB. Lateral Translation of the Patella in MPFC Reconstruction: A Biomechanical Study of Three Approaches. Published online 2022. doi:10.1055/s-0041-1741549

43. Xue Z, Song G yang, Liu X, et al. Excessive lateral patellar translation on axial computed tomography indicates positive patellar J sign. *Knee Surgery, Sport Traumatol Arthrosc*. 2018;26(12):3620-3625. doi:10.1007/S00167-018-4897-3/METRICS

44. Borukhov I, Esposito CI, Ismailidis P, et al. The trochlear sulcus of the native knee is consistently orientated close to the sagittal plane despite variation in distal condylar anatomy. *Knee Surg Sports Traumatol Arthrosc*. Published online 2021. doi:10.1007/S00167-021-06667-9

45. Murphy A. Knee (lateral view). *Radiopaedia.org*. Published online November 14, 2019. doi:10.53347/RID-72198

46. Wang XM, Liu HX, Niu JH, Duan GM, Wang F. Relationship between the Patellar Ridge and the Femoral Trochlea in the Patellar Tracking. *Orthop Surg*. 2016;8(4):468-474. doi:10.1111/OS.12290

47. Tanaka MJ, Elias JJ, Williams AA, Demehri S, Cosgarea AJ. Characterization of patellar maltracking using dynamic kinematic CT imaging in patients with patellar instability. *Knee Surgery, Sport Traumatol Arthrosc*. 2016;24(11):3634-3641. doi:10.1007/S00167-016-4216-9/METRICS

48. Frings J, Dust T, Krause M, et al. Objective assessment of patellar maltracking with 3 T dynamic magnetic resonance imaging: feasibility of a robust and reliable measuring technique. *Sci Reports 2020 101*. 2020;10(1):1-13. doi:10.1038/s41598-020-72332-9

49. Rosa SB, Ewen PM, Doma K, Ferrer JFL, Grant A. Dynamic Evaluation of Patellofemoral Instability: A Clinical Reality or Just a Research Field? A Literature review. *Orthop Surg*. 2019;11(6):932-942. doi:10.1111/OS.12549

50. Servien E, Ait Si Selmi T, Neyret P. [Study of the patellar apex in objective patellar dislocation]. *Rev Chir Orthop Reparatrice Appar Mot*. 2003;89(7):605-612.

51. Dickschas J, Harrer J, Bayer T, Schwitulla J, Strecker W. Correlation of the tibial tuberosity-trochlear groove distance with the Q-angle. *Knee Surg Sports Traumatol Arthrosc*. 2016;24(3):915-920. doi:10.1007/S00167-014-3426-2

52. Loudon JK. BIOMECHANICS AND PATHOMECHANICS OF THE PATELLOFEMORAL JOINT. *Int J Sports Phys Ther*. 2016;11(6):820. Accessed May 10, 2023. /pmc/articles/PMC5095937/

53. Hayat Z, Bitar Y El, Case JL. Patella Dislocation. *StatPearls*. Published online July 4, 2022. Accessed May 10, 2023. https://www.ncbi.nlm.nih.gov/books/NBK538288/

54. Wallace DA, Salem GJ, Salinas R, Powers CM. Patellofemoral joint kinetics while squatting with and without an external load. *J Orthop Sports Phys Ther*. 2002;32(4):141-148. doi:10.2519/JOSPT.2002.32.4.141

Appendix A; extra visualization of results Ch. 3

	Healthy vs PFI	Healthy vs Unaffected	Healthy vs Affected	Affected vs unaffected
Trochlea-patella distance	1, 3-7, 9-20, 22-60, 62-70, 73, 88-90, 92, 97	1, 2-5, 7, 9, 12, 14, 16, 18, 20, 22-70, 74, 75, 88, 97	1, 3, 6, 7, 9-11, 14-17, 19, 20, 22, 23, 25, 26, 29-38, 39-52, 54, 56, 57, 73, 88, 90, 91	none

Table 1. Overview of parts of the trochlear groove where a statistical difference is present.

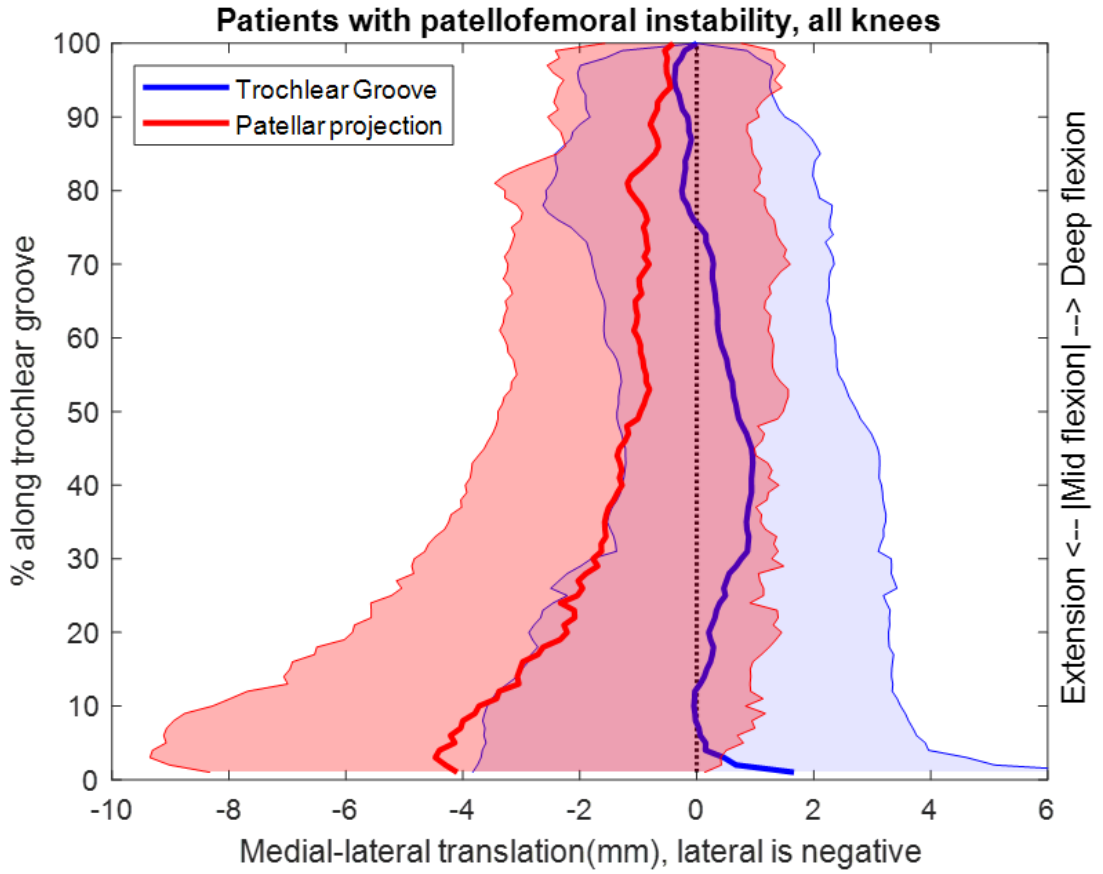

Figure 1.Overview of the mean trochlear rollout, and its standard deviation, of patients with PFI

Appendix B; Matlab script for the general pre-processing steps

Matlab script for the pre-processing steps, used for both chapter 2 and 3

```
clearvars
close all
clc

addpath(genpath('C:\users\z852332\Documents\MATLAB'));
main_folder = 'C:\Users\z852332\Documents\MATLAB\Data\4DCTHK_RAD_001';      %
adjust to dataset number
%load 'C:\users\z852332'\Documents\MATLAB\Data_patients_PFI\PFI_021\meshes.mat;
folder_static_mask = join([main_folder,'/mask/static/T_0.mha']);
folder_dynamic_mask = join([main_folder,'/mask/dynamic']);
folder_static_mha = strrep(folder_static_mask, 'mask', 'mha');
folder_dynamic_mha = strrep(folder_dynamic_mask, 'mask', 'mha');

frms = 39;
bns = {'fem','pat','tib'};
side ={'left','right'};

%% Check and load if registration is performed, or perform registration
    if ~exist(fullfile(main_folder, 'workspace_final.mat'),'file')
    if ~exist(fullfile(main_folder, 'transref.mat'),'file')
    if ~exist(fullfile(main_folder,'transforms'),'dir')

% Point cloud
pc_register(folder_static_mask,folder_dynamic_mask,main_folder)

% CPD
run_elastix_pcinput_vol(main_folder,folder_static_mha,folder_static_mask,folder_dy
namic_mha,folder_dynamic_mask)

    elseif exist(fullfile(main_folder,'transforms'),'dir')
           load(join([main_folder,'/meshes.mat']));
    end

% Elastix to matlab transformation matrix
            pathparfiles = main_folder;
            pathmask = join([main_folder,'/mask']);
            [tf,tf_prim,bones,secrot] =
extract_rotation_from_tffile_singlemesh(pathparfiles,pathmask);

% Transformation of static scans, and ERC reference frames
            applyTransform =  @(v,t) v*t.T + t.c(1,:);
            transformed_bones = [];
            refFrames = [];

for fr = 1:frms
for sd = 1:length(side)
for bn = 1:length(bns)
    transformed_bones.(bns{bn}).(side{sd}){fr}.V =
applyTransform(bones.(bns{bn}).(side{sd}).vertices,tf.(bns{bn}).(side{sd}){fr});
    transformed_bones.(bns{bn}).(side{sd}){fr}.F =
bones.(bns{bn}).(side{sd}).faces;
end

% Create estimate references frames
    axEst = calculateExternalFrame(transformed_bones.fem.(side{sd}){fr}.V,...
```

```
transformed_bones.pat.(side{sd}){fr}.V,transformed_bones.tib.(side{sd}){fr}.V);
    [refFrame,stlData,DiagInfo] =
ERCkneeReferenceFrames(transformed_bones.fem.(side{sd}){fr},...

transformed_bones.pat.(side{sd}){fr},transformed_bones.tib.(side{sd}){fr},axEst);
    refFrames.(side{sd}){fr} = refFrame;
    clearvars refFrame
end
end
%
% Transformed static scans + refframes
    save(fullfile(main_folder,'transref.mat'))

elseif exist(fullfile(main_folder, 'transref.mat'),'file')
       load(join([main_folder,'/transref.mat']));
    end

% Interpolate per angle
    [Transform, Angles,TfAngs,FlexI,ExtI] = interpolaterottrans(tf,bones);

%% Flexie/extensie, varus/valgus, endo/exo
[TKin] = findTFAngles(bones,Transform);

Ang_original = [];
for sd = 1:2
    for i = 1:frms
fem.V = bones.fem.(side{sd}).vertices;
fem.F = bones.fem.(side{sd}).faces;

tib.V = bones.tib.(side{sd}).vertices;
tib.F = bones.tib.(side{sd}).faces;

pat.V = bones.pat.(side{sd}).vertices;
pat.F = bones.pat.(side{sd}).faces;

[ref,dat,info] = ERCkneeReferenceFrames(fem,pat,tib);

fwdref = @(v,tr) v*tr.T;

    f = fwdref([ref.f.X;ref.f.Y;ref.f.Z],tf.fem.(side{sd}){i});
    t = fwdref([ref.t.X;ref.t.Y;ref.t.Z],tf.tib.(side{sd}){i});
    Ang_original.(side{sd})(i,1:3) = findang(f,t);

    end
end

% Transformed dynamic scans + refframes
    save(fullfile(main_folder,'workspace_final.mat'))

elseif exist(fullfile(main_folder, 'workspace_final.mat'),'file')
       load(join([main_folder,'/workspace_final.mat']));
       load(join([main_folder,'/meshes.mat']));
    end


%% Visualization
[Transformed_static, Initial_dynamic] =
visualization(frms,bns,side,sd,transformed_bones,dyn,refFrames);
```

Appendix C; matlab script Ch. 2

Matlab script for Chapter 2

```
clc
clearvars
addpath(genpath('C:\users\z852332\Documents\MATLAB'));

folder = 'C:\Users\z852332\Documents\MATLAB\Data_patients_PFI\PFI_020';
% Change to correct scan
mkdir(folder,'temp');
addpath(fullfile(folder,'temp'));

%% read mesh
load('C:\Users\z852332\Documents\MATLAB\Data_patients_PFI\PFI_020\meshes.mat')
% Change to correct scan
mesh = stat.left.fem; %% Get femurmesh

% Determine refframe
F.V = mesh.vertices;
F.F = mesh.faces;

axEst.X = [ 0 -1 0];
axEst.Y = [ 0  0 1];
axEst.Z = [-1  0 0];

[ref,stl,diag] = ERCkneeReferenceFrames(F,[],[],axEst);

TR =[0,-1,0;0,0,1;-1,-0,0];%% rotate back towards other axis (wcs orientation).
Prevents swap of views.
RotPoint = ref.f.origin; % defines rotationpoint

% 'add' rotation around world axis
radang = deg2rad(10);
AddR = euler2rotMat(0, 0, 0); % if all are zero no rotation added -> lateral view
% be aware, rotation is in WORLDCS.

FinRot = [ref.f.X;ref.f.Y;ref.f.Z]'*TR*AddR;

FinTrans = [ref.f.origin]*FinRot; %% final translation to place femorigin on
origin

% Write transformfile
tfmfile = fullfile(folder,'temp','tfm.txt');
maketf(FinRot,FinTrans,RotPoint,tfmfile);

% viz, use to check
figure
pcshow((mesh.vertices-ref.f.origin)*([ref.f.X;ref.f.Y;ref.f.Z]'*TR),'r');
hold on
pcshow((mesh.vertices-ref.f.origin)*FinRot,'b');
plotCoords();

%% Run python file
pythonexe = 'C:\Program files\Python\pythonw.exe';

pyfile =
'C:\Users\z852332\Documents\MATLAB\Patella_alta\Projections\Rotatevolume.py';
```

```
inpath =
'C:\Users\z852332\Documents\MATLAB\Data_patients_PFI\PFI_020\static\T_0.mha';
% Change to correct folder
outpath =
'C:\Users\z852332\Documents\MATLAB\Data_patients_PFI\PFI_020\temp\static_true_late
ral.mha';              % Change to correct folder
sep = '"';

%Make sure all slashes are correclty directed for python
pythonexe(strfind(pythonexe,'\'))='/';
pyfile(strfind(pyfile,'\'))='/';
tfmfile(strfind(tfmfile,'\'))='/';
inpath(strfind(inpath,'\'))='/';
outpath(strfind(outpath,'\'))='/';

% Execute the rotatevolume script
cmdf = strcat(sep,pythonexe,sep," ",...
    sep,pyfile,sep," ",sep,inpath,sep," ",sep,outpath,sep," ",sep,tfmfile,sep);
tic
system(cmdf);
toc %elaspsed time

%% Get volume
[vol, meta, ctr, PixSz] = Centre_mha(outpath);

%% Get ROI (patella region)
for sd = 1 %Specify side of interest
    if side{sd} == "right"
        roix = (1:floor(0.5*meta.Dimensions(1)));
    elseif side{sd} == "left"
        roix = floor(0.5*meta.Dimensions(1)+1):meta.Dimensions(1);

    end
end

roiy = floor(0.3*meta.Dimensions(2)):floor(0.7*meta.Dimensions(2));
% Statische scan
roiz = floor(0.25*meta.Dimensions(3)):floor(0.75*meta.Dimensions(3));
% Statische scan
volroi = vol(roix,roiy,roiz);          % Statische scan
ctrroi{1}=ctr{1}(roix);                % Statische scan
ctrroi{2} = ctr{2}(roiy);              % Statische scan
ctrroi{3} = ctr{3}(roiz);              % Statische scan

% roiy = floor(0.1*meta.Dimensions(2)):floor(0.5*meta.Dimensions(2));
% Dynamische scan
% volroi = vol(roix,roiy,:);           % Dynamische scan
% ctrroi{1}=ctr{1}(roix);              % Dynamische scan
% ctrroi{2} = ctr{2}(roiy);            % Dynamische scan
% ctrroi{3} = ctr{3};                  % Dynamische scan

%%
depthDetail = PixSz;
angs = [0,90,0]; % hier kun je met de hoeken spelen. [0,90,0] is 'zuiver lateraal'
imprj = ct22d(volroi,ctrroi,angs,PixSz,depthDetail); % bereken intensity proj.


figure
imshow(mat2gray(rot90(imprj)));
```

```
hold on
colorbar()
%caxis([0.5 1])                  % Dynamische CAXIS, bij statische scan geen caxis
gebruiken, en bij ab/ad 0.3 als startpunt gebruiken
% Point selection
[xi,yi] = getpts;

Points =[];
Points(1,:) = xi;
Points(2,:) = yi;

p1 = Points(:,1);
p2 = Points(:,2);
p3 = Points(:,3);
p4 = Points(:,4);
p5 = Points(:,5);
p6 = Points(:,6);

dB = norm(p1-p2);
dA = norm(p2-p3);
dC = norm(p5-p6);
dD = norm(p4-p5);
insall = dA/dB;
caton = dC/dD;
```

Appendix D; matlab script Ch. 3

Matlab script used for chapter 3

```
close all
clearvars
clc

addpath(genpath('C:\Users\z852332\Documents\MATLAB'))
noPoints = 100;
Main_folder = 'C:\Users\z852332\Documents\MATLAB\workspaces\PFI';
files = dir(fullfile(Main_folder,'**','*space.mat'));
%%
for n = 21
noPoints = 100;
Main_folder = 'C:\Users\z852332\Documents\MATLAB\workspaces\PFI';
files = dir(fullfile(Main_folder,'**','*space.mat'));
subfile = files(n).folder
load(join([subfile,'/workspace.mat']));
sd = 1

F.V  = bones.fem.(side{sd}).V;
F.F  = bones.fem.(side{sd}).F;
P.V  = bones.pat.(side{sd}).V;
P.F = bones.pat.(side{sd}).F;
T.V  = bones.tib.(side{sd}).V;
T.F = bones.tib.(side{sd}).F;

[CSDATA.(side{sd}),STLDATA.(side{sd}),DIAGDATA.(side{sd})] =
ERCkneeReferenceFrames(F,P,T);

worldF.vertices = (F.V-CSDATA.(side{sd}).f.origin)*...
    [CSDATA.(side{sd}).f.X;CSDATA.(side{sd}).f.Y;CSDATA.(side{sd}).f.Z]';
worldF.faces= F.F;

worldP.vertices = (P.V-CSDATA.(side{sd}).f.origin)*...
    [CSDATA.(side{sd}).f.X;CSDATA.(side{sd}).f.Y;CSDATA.(side{sd}).f.Z]';
worldP.faces= P.F;

worldT.vertices = (T.V-CSDATA.(side{sd}).f.origin)*...
    [CSDATA.(side{sd}).f.X;CSDATA.(side{sd}).f.Y;CSDATA.(side{sd}).f.Z]';
worldT.faces= T.F;

% vind hoogste punt waar TG / condyle begint
%Find the articulating surfaces according to the WCS
worldFcondyle1 = (DIAGDATA.(side{sd}).f.sections.articulatingSurface1.V-
CSDATA.(side{sd}).f.origin)*...
    [CSDATA.(side{sd}).f.X;CSDATA.(side{sd}).f.Y;CSDATA.(side{sd}).f.Z]';

worldFcondyle2 = (DIAGDATA.(side{sd}).f.sections.articulatingSurface2.V-
CSDATA.(side{sd}).f.origin)*...
    [CSDATA.(side{sd}).f.X;CSDATA.(side{sd}).f.Y;CSDATA.(side{sd}).f.Z]';

%Check
worldP1 = (DIAGDATA.(side{sd}).f.points12.pt1-CSDATA.(side{sd}).f.origin)*...
    [CSDATA.(side{sd}).f.X;CSDATA.(side{sd}).f.Y;CSDATA.(side{sd}).f.Z]';


maxYStart = max([worldFcondyle1(:,2);worldFcondyle2(:,2)]); %Heighest point
minXEnd = min([worldFcondyle1(:,2);worldFcondyle2(:,2)]);
```

```
tE= opcodemesh(worldF.vertices',worldF.faces'); %collission detection
fromStart = [0 maxYStart 0];
[~,~,~,~,hitsStart] = tE.intersect(fromStart',[100 0 0]');
radius = rssq(hitsStart);
angleIn = atan(hitsStart(1)/hitsStart(2));


% from
% snijd world femur over z (=y femcoors) op 000
onelist = ones(length(worldF.vertices));

cplane = [0 0 0 0 0 1];
    cut = plane2iplane(cplane);
[crossection,~,pairscros,cutFcros]=qmeshcut(worldF.faces,worldF.vertices,onelist,c
ut);
% figure
% scatter(crossection(:,1),crossection(:,2))
% axis equal
[~, indmaxX] = max(crossection(:,1)); %this could be start of trochlea
[~, indminY] = min(crossection(:,2)); %end of trochlea?
[~, indminX] = min(crossection(:,1)); %?
% circlefit met minimaal de punten tussen worldP1 en indmax
% welke punnten liggen hiertussen?
sulcus =
find(crossection(:,1)<crossection(indmaxX,1)&crossection(:,1)>crossection(indminY,
1) &...

crossection(:,2)>crossection(indminY,2)&crossection(:,2)<crossection(indmaxX,2));
xy = [crossection(sulcus,1),crossection(sulcus,2)];
Par = CircleFitByPratt(xy);

[rij, kolom] =knnsearch(crossection,hitsStart');

% make blumensaatline
% ligt deze tussen minX & minY?

[BlumensaatPointsI,~] = find(crossection(:,2)>crossection(indminY,2)&...
    crossection(:,2)<crossection(indminX,2)&...
    crossection(:,1)>crossection(indminX,1)&...
    crossection(:,1)<crossection(indminY,1));

% fit line through these points

Bsat = [crossection(BlumensaatPointsI,1),crossection(BlumensaatPointsI,2),...
    crossection(BlumensaatPointsI,3)];
BsatO = [crossection(BlumensaatPointsI,1),crossection(BlumensaatPointsI,2),...
    crossection(BlumensaatPointsI,3)];
counter = 1;
yn =1;
%
while yn
    [lineOut] = lsLine(BsatO);
    D =distancePointLine(Bsat,lineOut);
    TF{counter} = isoutlier(D);
    BsatO = Bsat(TF{counter}==0,:);
    if counter~= 1
    if isequal(TF{counter},TF{counter-1}) || counter > 10
```

```
        yn=0;
    end
    end
    counter = counter+1;
end

%intersect blumensaat & sulcuscircle

lineOut2d = lineOut([1,2,4,5]);
intersectpoint = intersectLineCircle(lineOut2d,[Par(1),Par(2),Par(3)]);
[~,minintersect] = min(intersectpoint(:,2));
intersectpoint = intersectpoint(minintersect,:);

%new circlepoints =

sulcus2I = find(crossection(:,2)<hitsStart(2)&...
    crossection(:,2)>intersectpoint(2)&...
    crossection(:,1)>intersectpoint(1));

%fitnewcircle

newXY = [crossection(sulcus2I,[1,2])];
ParTwo = CircleFitByPratt(newXY);

% meest grote y punt op sulcusarc

[~,indMaxSulc]= max(crossection(sulcus2I,2));

[rxS,clS]= min(abs(crossection(sulcus2I,2)-ParTwo(2)));

startPointofSulcus = crossection(sulcus2I(clS),:); %moet recht boven

[val,indMinSulc]= min(crossection(sulcus2I,1));

endPointofSulcus =crossection(sulcus2I(indMinSulc),:);
% calculate angle with respect to par 2

dXstart = startPointofSulcus(1)-ParTwo(1);
dYstart = startPointofSulcus(2)-ParTwo(2);

dXend = endPointofSulcus(1)-ParTwo(1);
dYend = endPointofSulcus(2)-ParTwo(2);

startAngle = atan2(dYstart,dXstart);

endAngle = atan2(dYend,dXend);

radiansAng = startAngle +linspace(0,endAngle-startAngle,10);

starthoek  = atan2(startPointofSulcus(2)-ParTwo(2),startPointofSulcus(1)-
ParTwo(1));
endhoek = atan2(endPointofSulcus(2)-ParTwo(2),endPointofSulcus(1)-ParTwo(1));

endhoek_1 = endhoek +0.05;
starthoek_1 = starthoek - 0.05;
angleDifference =mod(endhoek_1-starthoek_1,2*pi);

if angleDifference > pi
    angleDifference1 = 2*pi-angleDifference;
```

```
else angleDifference1=angleDifference;
end

radiansAng = starthoek -linspace(0,angleDifference1,100);

circCoordinates = [cos(radiansAng)',sin(radiansAng)'].*60 + ParTwo(1:2);

% line fit over punten tussen ind min

normCircs =[circCoordinates(:,1),circCoordinates(:,2)]./60;

for i = 1:length(normCircs)
    %create normal 2 cutting plane
    d = null([normCircs(i,1) normCircs(i,2) 0])';
    cplane = [ParTwo(1) ParTwo(2) 0 d(1,1) d(1,2) d(1,3)];
    rAng = signedAngleTwo3DVectors([d(1,1) d(1,2) d(1,3)],[0 1 0],[0 0 1],0);
    cut = plane2iplane(cplane);
    %cut mesh
    [vs{i},~,pairs,cutF]=qmeshcut(worldF.faces,worldF.vertices,onelist,cut);
    [vs_2{i},pairsU{i},cutFacesU{i},polys{i}] =
simplifyQmeshcuts(vs{i},pairs,worldF.faces,....
        worldF.vertices,cutF);

    rotm = euler2rotMat(0, 0, rAng);

    vs_rotated{i} = (vs_2{i}-[ParTwo(1) ParTwo(2) 0])*rotm';

    %convhull of this shape
    hull = convhull(double([vs_rotated{i}(:,1),vs_rotated{i}(:,3)]));
    %all points again
    points = [vs_rotated{i}(:,1),vs_rotated{i}(:,3)];
    % hullpoints --> coordinates
    hullPoints = [vs_rotated{i}(hull,1),vs_rotated{i}(hull,3)];
    %select right part
    K= 0 < hullPoints(:,1);
    RS=K(1:end-1)& K(2:end); % == right side -->
    %find distance between points on convhull
    difconv = rssq(diff(hullPoints),2);
    [~,indexlargestdiff] = sort(abs(difconv).*RS,'descend');
    % determine 'edgepoints'
    pclp1 = hull(indexlargestdiff(1)+1);
    pclp2 = hull(indexlargestdiff(1));

    cdp1P = find(cell2mat(polys{i}) == pclp1) ;
    cdp2P = find(cell2mat(polys{i}) == pclp2) ;

    if cdp1P > cdp2P
        tmp = cdp1P ;
        cdp1P = cdp2P ;
        cdp2P = tmp ;
    end
    if cdp2P(1) == 1
        cdp2P(1) = [];
    end
    convI = circshift(cell2mat(polys{i}),-(cdp1P-1)); %make starting I.

    shiftPoints = vs_rotated{i}(convI,:);

    Tlength = cdp2P - cdp1P +1;
```

```
    %two paths

    pointsCCW = [shiftPoints(1:Tlength,1),shiftPoints(1:Tlength,3)];
    pointsCW = [shiftPoints([Tlength:length(shiftPoints),1],1),...
        shiftPoints([Tlength:length(shiftPoints),1],3)];

    lengthCirc(1) = sum(rssq(diff(pointsCCW),2));
    lengthCirc(2) = sum(rssq(diff(pointsCW),2));

    [len(i),indexminimum] = min(lengthCirc);
    if indexminimum ==1
        TGpoints = pointsCCW;
    else
        TGpoints = pointsCW;
    end

    Tlength = cdp2P - cdp1P +1;
    tbit = vs_rotated{i}(convI(1:Tlength),:); % points between edgepoints or
tgpoints
    tbit2d = TGpoints;

    for p = 2 : size(tbit2d,1)-1
        lineL{p} = createLine(tbit2d(1,:),tbit2d(p,:));
        lineR{p} = createLine(tbit2d(p,:),tbit2d(end,:));
        distL{p} = distancePointLine(tbit2d, lineL{p}) ;
        distR{p} = distancePointLine(tbit2d, lineR{p});
        err = min(distL{p},distR{p});
        errorL2(p) = rssq(err);
    end

    errorL2(1) = inf ;
    [~,TGIndex{i}] = min(errorL2);

    tgpoint = intersectLines(lineL{TGIndex{i}}, lineR{TGIndex{i}});

    TG{i} = [tgpoint(1),0,tgpoint(2)]...
        *rotm+[ParTwo(1) ParTwo(2) 0];

    EdgeL{i} = [tbit(end,1),tbit(end,2),tbit(end,3)]*rotm+[ParTwo(1) ParTwo(2)
0];%+[ParTwo(1) ParTwo(2) 0];;
    EdgeR{i} = [tbit(1,1),tbit(1,2),tbit(1,3)]*rotm+[ParTwo(1) ParTwo(2)
0];%+[ParTwo(1) ParTwo(2) 0];;

    if EdgeL{i}(3)>EdgeR{i}(3)
        tE = EdgeR{i};
        EdgeR{i} = EdgeL{i};
        EdgeL{i} = tE;
    end
end


%% Determine intersection points patella --> femur
for i = 1:length(Angles.(side{sd}))
    RM_F = quatern2rotMat(Transform.fem.(side{sd}).Q(i,:));
    trans_F = Transform.fem.(side{sd}).t(i,:);
F_dyn.V = bones.fem.(side{sd}).V*RM_F + trans_F;
F_dyn.F = bones.fem.(side{sd}).F;
origin_femur_dyn = CSDATA.(side{sd}).f.origin*RM_F + trans_F;
```

```
RM_P = quatern2rotMat(Transform.pat.(side{sd}).Q(i,:));
    trans_P = Transform.pat.(side{sd}).t(i,:);
P_dyn.V = bones.pat.(side{sd}).V*RM_P + trans_P;
P_dyn.F = bones.pat.(side{sd}).F;
origin_patella_dyn = CSDATA.(side{sd}).p.origin * RM_P + trans_P;

RM = quatern2rotMat(Transform.tib.(side{sd}).Q(i,:));
    trans = Transform.tib.(side{sd}).t(i,:);
T_dyn.V = bones.tib.(side{sd}).V*RM + trans;
T_dyn.F = bones.tib.(side{sd}).F;


% transformation to world coordinates --> based on reference frames of femur
worldF_dyn.vertices = (F_dyn.V-CSDATA.(side{sd}).f.origin)*...
    [CSDATA.(side{sd}).f.X;CSDATA.(side{sd}).f.Y;CSDATA.(side{sd}).f.Z]';
worldF_dyn.faces= F_dyn.F;
origin_femur_wcs = (origin_femur_dyn-CSDATA.(side{sd}).f.origin)*...
    [CSDATA.(side{sd}).f.X;CSDATA.(side{sd}).f.Y;CSDATA.(side{sd}).f.Z]';

worldP_dyn.vertices = (P_dyn.V-CSDATA.(side{sd}).f.origin)*...
    [CSDATA.(side{sd}).f.X;CSDATA.(side{sd}).f.Y;CSDATA.(side{sd}).f.Z]';
worldP_dyn.faces= P_dyn.F;
origin_patella_wcs = (origin_patella_dyn-CSDATA.(side{sd}).f.origin)*...
    [CSDATA.(side{sd}).f.X;CSDATA.(side{sd}).f.Y;CSDATA.(side{sd}).f.Z]';

worldT_dyn.vertices = (T_dyn.V-CSDATA.(side{sd}).f.origin)*...
    [CSDATA.(side{sd}).f.X;CSDATA.(side{sd}).f.Y;CSDATA.(side{sd}).f.Z]';
worldT_dyn.faces= T_dyn.F;

line = createLine3d(origin_patella_wcs,origin_femur_wcs);
intersection = intersectLineMesh3d(line,worldF_dyn.vertices,worldF_dyn.faces);
if isempty(intersection) == 1
    intersection_point_stat_WCS(i,:) = [0,0,0];
    continue
end

if intersection(1,1)>intersection(2,1)
    intersection_point = intersection(1,:);
else intersection_point = intersection(2,:);
end
% dynamic WCS --> static WCS
intersection_point_dyn_SCS = intersection_point
*[CSDATA.(side{sd}).f.X;CSDATA.(side{sd}).f.Y;CSDATA.(side{sd}).f.Z] +
CSDATA.(side{sd}).f.origin;
intersection_point_stat_SCS = (intersection_point_dyn_SCS - trans_F) * RM_F';
intersection_point_stat_WCS(i,:) = (intersection_point_stat_SCS -
CSDATA.(side{sd}).f.origin)*...
    [CSDATA.(side{sd}).f.X;CSDATA.(side{sd}).f.Y;CSDATA.(side{sd}).f.Z]';
end
%%
for k = 1:length(intersection_point_stat_WCS)
patdXend = intersection_point_stat_WCS(k,1)-ParTwo(1);
patdYend = intersection_point_stat_WCS(k,2)-ParTwo(2);
patAngle(k) = atan2(patdYend,patdXend);
angle_difference = abs(radiansAng-patAngle(k));
[closest_angle(k),index_closest_angle(k)] = min(angle_difference);
original_angle(k) = radiansAng(index_closest_angle(k));
used_angle_diff(k) = angle_difference(index_closest_angle(k));
```

```
end

spacing = (radiansAng(1)-radiansAng(2))/2;
%% visualize endproduct
figure()
patch(worldF,'FaceAlpha',0.2,'EdgeAlpha',0.1,'FaceColor','g','EdgeColor','none');
axis equal; rotate3d on;
hold on
%
for i =1:noPoints
   pcshow(vs_2{i},'b');
   tg = scatter3(TG{i}(:,1),TG{i}(:,2),TG{i}(:,3),30,'go','filled');
   l = scatter3(EdgeL{i}(:,1),EdgeL{i}(:,2),EdgeL{i}(:,3),30,'co','filled');
   m = scatter3(EdgeR{i}(:,1),EdgeR{i}(:,2),EdgeR{i}(:,3),30,'mo','filled');
end


hold on
for k = 1:length(intersection_point_stat_WCS)
p =
plot3(intersection_point_stat_WCS(k,1),intersection_point_stat_WCS(k,2),intersecti
on_point_stat_WCS(k,3),"*r",'MarkerSize',10);
end
ylim([-23 60])
campos([552 -433 154])
legend([tg,l,m,p],'Trochlear groove','Lateral condyle','Medial condyle','Patellar
projection point','color','white')
%% 2D visualization
ldist =zeros(100,1);
mdist =zeros(100,1);
tgdist = zeros(100,1);
pdist = zeros(length(intersection_point_stat_WCS),2);
for i =1:100
    if sd == 1;
    ldist(i) = EdgeL{i}(3);
    mdist(i) = EdgeR{i}(3);
    tgdist(i) = TG{i}(3);
    else
    ldist(i) = -EdgeR{i}(3);
    mdist(i) = -EdgeL{i}(3);
    tgdist(i) = -TG{i}(3);
    end
end

for k = 1:length(intersection_point_stat_WCS)
    if (used_angle_diff(k) > spacing && index_closest_angle(k) == 1) ||
(used_angle_diff(k) > spacing && index_closest_angle(k) == 100)
        continue
    end
    pdist(k,2) = index_closest_angle(k);
    if sd == 1
    pdist(k,1) = intersection_point_stat_WCS(k,3);
    else
    pdist(k,1) = -intersection_point_stat_WCS(k,3);
    end
end
%%
for i = 1:100
    tgdist_new(i) = tgdist(i)-tgdist(100);
```

```
end
for k = 1:length(pdist)
    pdist_new(k,1) = pdist(k,1)-tgdist(100);
    pdist_new(k,2) = pdist(k,2);
end
%%
figure
hold on
l = plot(smooth(ldist),1:100,'b');
plot([0 0],[1 100],'k:');
hold on
m = plot(smooth(mdist),1:100,'m');
% plot(smooth(tgdist),1:100,'r')
tg = plot(smooth(tgdist_new),1:100,'k');
hold on
for k = 1:length(pdist)
    if pdist(k,2) == 0
        continue
    end
% scatter(pdist(k,1),pdist(k,2),'c')
p = scatter(pdist_new(k,1),pdist_new(k,2),'g')
end
axis equal
legend([l,m,tg,p],'Lateral condyle','Medial condyle','Trochlear groove','Patellar
projection point')
title('Rollout of both condyles and the trochlear groove')
xlabel('Medial-lateral translation (mm)')
ylabel('% along the trochlear groove')
xlim_1=get(gca,'XLim');
ylim_1=get(gca,'YLim');
ht = text(0.1*xlim_1(1)+1.18*xlim_1(2),1.75*ylim_1(1)+0.05*ylim_1(2),'Extension <-
- |Mid flexion| --> 90 degrees flexion');
set(ht,'Rotation',90)
set(ht,'FontSize',11)

%Results
% results_PFI_left.scan{n}.pdist = pdist_new;
% results_PFI_left.scan{n}.ldist = ldist;
% results_PFI_left.scan{n}.mdist = mdist;
% results_PFI_left.scan{n}.tgdist = tgdist_new;
%     clearvars -except results_PFI_left
end
```